

ABSTRACT

Title of Thesis: MOLECULAR SIMULATION OF
ANTIMICROBIAL PEPTIDE WLBU2-MOD
BINDING WITH GRAM-NEGATIVE INNER
MEMBRANE MIMIC

Tyler Cline, Master of Science, 2019

Thesis directed by: Associate Professor, Dr. Jeffery Klauda,
Chemical and Biomolecular Engineering

Since the discovery of Penicillin in 1928 by Sir Alexander Fleming, antibiotics have been one of the most important technologies in modern medicine. Due to the lack of novel innovative methods and the gross abuse of antibiotics both in human use and agriculture, we currently face an antibiotic resistance crisis. In the last fifty years only a handful of new class of antibiotics that target gram-positive bacteria have been introduced and, in that time, no new class of antibiotics that target gram-negative bacteria have been introduced. This thesis focuses on the molecular dynamic simulations involving the cationic α -helical antibacterial peptide, WLBU2-mod (RRWVRRVRRVWRRVVRVRRWVRR), binding with a gram-negative bacterial inner membrane (IM) mimic composed of palmitoyloleoyl PE (POPE), palmitoyloleoyl PG (POPG), and 1,1',2,2'-tetraoctadecenoyl CL (TOCL2) in a 7:2:1 ratio respectively. The structure of WLBU2-mod was predicted using Robetta to be either a single extended α -helical structure or a bent α -helical structure. Replica exchange with solute tempering with an improved Hamiltonian acceptance protocol (REST2) was performed on WLBU2-mod to relax the peptide to an unstructured conformation in an

explicit aqueous solution. WLBU2-mod relaxed with REST2 consists of mainly random coil and β -sheet secondary structure which matches experimental circular dichroism (CD) results collected by Aria Salyapongse and Dr. Tristram-Nagle. Experimental CD results with the IM predicted the peptide to be structured with majority α -helical secondary structure, contrary to the unstructured results of the peptide in water. Both structured and unstructured WLBU2-mod were placed in parallel 10 Å above the IM mimic and molecular dynamics (MD) was performed to observe the binding mechanism. Simulations failed to see significant bilayer thinning or penetration into the hydrophobic core but there is strong indication that our simulations represent in intermediate state toward the final binding mechanism. In order to observe more substantial binding to the IM, future projects should consider increasing the length of the simulations and flipping the orientation of the peptide to have the hydrophobic components face inward toward the bilayer. Future projects in combination with the groundwork laid out here will hopefully provide insight into how antibacterial peptides can become the answer to the resistance crisis we face today.

MOLECULAR SIMULATION OF ANTIMICROBIAL PEPTIDE WLBU2-
MOD BINDING WITH GRAM-NEGATIVE INNER MEMBRANE
MIMIC

by

Tyler Cline

Thesis submitted to the Faculty of the Graduate School of the
University of Maryland, College Park in partial fulfillment
of the requirements for the degree of
Master of Science
2019

Advisory Committee:

Dr. Jeffery Klauda, Chair

Dr. Amy Karlsson, Assistant Professor

Dr. Ganesh Sriram, Assistant Professor

© Copyright by
Tyler Cline
2019

Acknowledgments

I have worked on this project for the last two years and I would like to use this opportunity to acknowledge some of the people who have helped me get to this point. First and foremost, I would like to thank Dr. Jeffery Klauda who has been profoundly insightful, positively inspirational, and extremely supportive throughout the entire project. Dr. Klauda's mentorship has been an invaluable learning opportunity for me, not just for this project, but for the rest of my career. I would like to also acknowledge our collaborator Dr. Tristram-Nagle who has shown me great professionalism and patience as I learned on the job and often asked, what I imagine was deemed, "dumb questions". Without Dr. Tristram-Nagle's undying support and efforts, there would be no project to begin with. I would also like to acknowledge the entire team and anyone else who provided research efforts toward this project including Aria Salyapongse, Dr. Anja Penk, Dr. Daniel Huster, and Dr. JC Gumbart. Finally, I would like to thank the committee members who have provided me with excellent questions and support as I finalized my thesis. Drs. Sriram and Karlsson's insightful criticism allowed me to improve my understanding of how to write an excellent professional paper. Without the support of all the people who sacrificed their time toward this project, none of this would be possible. To each and every one of you, thank you.

TABLE OF CONTENTS

LIST OF TABLES	iv
LIST OF FIGURES	v
LIST OF ABBREVIATIONS.....	viii
CHAPTER 1: INTRODUCTION	1
1.1 Background of Antimicrobial Peptides.....	1
1.2 New Antibiotic Methods Needed.....	3
CHAPTER 2: METHODS.....	7
2.1 Protein Structure Prediction Using the Robetta ^{5,6} Server.....	7
2.2 WLBU2-mod Simulation Parameters	8
2.3 Membrane Simulation Parameters	10
2.4 IM with Parallel Inserted WLBU2-mod Simulation Parameters	11
CHAPTER 3: WLBU2-MOD PEPTIDE IN EXPLICIT AQUEOUS SOLUTION.....	13
3.1 WLBU2-mod Background and Robetta ^{5,6} Protein Structure Prediction	13
3.2 Brute-Force Molecular Dynamics.....	15
3.3 Replica Exchange with Solute Tempering (REST2).....	17
3.4 WLBU2-mod Analysis.....	20
CHAPTER 4: INNER MEMBRANE MIMIC OF GRAM-NEGATIVE BACTERIA....	28
4.1 Membrane Composition.....	28
4.2 Results of IM in Aqueous Solvent MD Simulations.....	30
CHAPTER 5: WLBU2-MOD PARALLEL INTRODUCTION WITH INNER MEMBRANE MIMIC	36
5.1 Results of Unstructured WLBU2-mod and IM.....	36
5.2 Results of Structured WLBU2-mod and IM	45
CHAPTER 6: FINAL COMMENTS.....	54
6.1 Summary of Thesis.....	54
6.2 Final Comments and Future Work	55
REFERENCES	58

LIST OF TABLES

Table 3.1 Four structures chosen for simulation with gram-negative bacterial IM mimic based on percent occurrence within equilibrated region resulting from REST2.

Table 3.2 Secondary structure breakdown of WLBU2 in water, pH 7.0, 310 K.

Table 4.1 Thickness data from equilibrated region of three all-atom control IM systems. Values reported as averages with standard error between the three replicas.

LIST OF FIGURES

Figure 1.1 Four structural classes typically found of antimicrobial peptides: α -helical, extended, mixed, and β -sheet. Examples of each class are shown in parenthesis below.

Figure 1.2 (a) Barrel-Stave Model showing perpendicular introduction of the AMP into the membrane forming water permeable pores within the membrane structure. (b) Carpet Model exhibiting parallel introduction of the AMP into the membrane forming micelle-like chunks of lipids causing the membrane structure to breakdown. (c) Toroidal Model with perpendicular introduction and mechanistic features like the Barrel-Stave Model, however the pores are composed of both the AMP and hydrophilic lipid head groups. Original figure 3,4,5 used with permission.

Figure 1.3 Antibiotic prescriptions in the United States for every 1,000 persons in 2010. Original figure 2 used with permission.

Figure 1.4 A timeline detailing antibiotic development and introduction shown with known antibiotic resistant strains identified. Over the last two decades the number of developed antibiotics introduced has stayed regular while the number of antibiotic resistant strains of bacteria has substantially increased. Original figure 1 used with permission.

Figure 3.1 (a) Straight α -helix WLBU2 (b) α -helix bent WLBU2 (c) Straight α -helix WLBU2-mod (d) α -helix bent WLBU2-mod. WLBU2 is composed of 13 Arg, 8 Val, and 3 Trp. Colored by residue type; non-polar (white) and polar (blue).

Figure 3.2 Brute force MD full trajectory time series after 200 ns for both double-helix and single-helix systems.

Figure 3.3 REST2 full trajectory time series after 150 ns for both double-helix and single-helix systems.

Figure 3.4 2-D contour plot for the RGY and number of residue contacts for (a) 0-100 ns of REST2 for double-helix system (b) 75-100 ns of REST2 for double-helix system (c) 0-100 ns of REST2 for single-helix system and (d) 75-100 ns of REST2 for single-helix system.

Figure 3.5 Ramachandran plots for REST2 for (a) double-helix (b) single-helix.

Figure 3.6 Experimental CD of 13 μ M WLBU2 in water. The difference between left and right circular polarized light is measured as the molar ellipticity and plotted against the wavelength of absorption. CD taken by Aria Salyapongse and analyzed by Aria Salyapongse and Dr. Tristram-Nagle.

Figure 4.1 (a) palmitoyloleoyl PE (POPE) (16:0,18:1) (b) palmitoyloleoyl PG (POPG) (16:0,18:1) (c) 1,1',2,2'-tetraoctadecenoyl CL (TOCL2) (18:1,18:1).

Figure 4.2 Gram-negative bacterial IM mimic consists of 50 lipids per leaflet composed of POPE (gray), POPG (blue), and TOCL2 (red) in a 7:2:1 ratio.

Figure 4.3 Surface area per lipid for 200 ns of brute force MD for the three all-atom IM replicas.

Figure 4.4 Chain order parameters for the sn-2 chain for POPE and POPG taken from the equilibrated region of the three all-atom IM replicas. Data taken as an average from the three replicas with the standard deviation shown as vertical error bars.

Figure 4.5 Chain order parameters for control POPE and POPG. Simulation data were re-ordered to match NMR assumption of monotonically decreasing order parameters. Simulation data taken from equilibrated region of the three all-atom IM replicas simulated at 303 K. Experimental data collected via NMR at 310 K by Drs. Anja Penk and Daniel Huster.

Figure 4.6 X-ray form factors for the gram-negative IM POPE:POPG:TOCL2 (7:2:1) control system without the peptide. Experimental results collected and analyzed by Aria Salyapongse and Dr. Tristram-Nagle at 310K. Simulations results collected using the equilibrated region of the IM MD simulations.

Figure 4.7 Electron density profile (EDP) for the bacterial IM in an explicit aqueous solvent.

Figure 5.1 HMMM binding mechanisms including initial placement (left) and after 200 ns of MD (right) for (a) system 1 (b) system 2 (c) system 3. Lipids shown without hydrogen and with the naming color scheme; carbon tail (gray) and phosphate headgroup (green). Peptide colored by residue; non-polar (white) and polar (blue).

Figure 5.2 Unstructured WLBU2-mod with all-atom IM after 150 ns of MD (a) system 1 (b) system 2 (c) system 3. Lipids shown without hydrogen and with the naming color scheme; carbon tail (gray) and phosphate headgroup (green). Peptide colored by residue; non-polar (white) and polar (blue).

Figure 5.3 Electron Density Profile for the three all-atom systems with unstructured WLBU2-mod and IM after 150 ns of MD simulation.

Figure 5.4 Chain order parameters for POPE and POPG with unstructured WLBU2-mod. Simulation data were re-ordered to match NMR assumption of monotonically decreasing order parameters. Simulation data taken from equilibrated region of the three all-atom IM replicas simulated at 303 K. Experimental data collected via NMR at 310 K by Drs. Anja Penk and Daniel Huster.

Figure 5.5 Ramachandran plots of the three all-atom systems with unstructured WLBU2-mod and IM after 150 ns of MD simulation.

Figure 5.6 Experimental CD of WLBU2 with the gram-negative IM. CD taken by Aria Salyapongse and analyzed by Aria Salyapongse and Dr. Tristram-Nagle.

Figure 5.7 HMMM binding mechanisms including initial placement (left) and after 150 ns of MD (right) for (a-c) double-helix (d-f) single-helix. Lipids shown without hydrogen and with the naming color scheme; carbon tail (gray) and phosphate headgroup (green). Peptide colored by residue; non-polar (white) and polar (blue).

Figure 5.8 Structured WLBU2-mod with all-atom IM after 150 ns of MD (a) double-helix (b) single-helix. Lipids shown without hydrogen and with the naming color scheme; carbon

tail (gray) and phosphate headgroup (green). Peptide colored by residue type; non-polar (white) and polar (blue).

Figure 5.9 Ramachandran plots of structured WLBU2-mod with the all-atom IM after 150-ns of MD.

Figure 5.10 EDP for all-atom IM with structured WLBU2-mod after 150 ns of MD simulation. The first EDP is shown for the double-helix (d) conformation and the second EDP is shown for the single-helix (s) conformation.

Figure 5.11 Electron density profile for the double-helix and single-helix structured WLBU2-mod with the IM. The dotted lines show where along the z-axis the maximum density for each structure occurs.

Figure 5.12 Form factors for MD simulations of double-helix and single-helix WLBU2-mod with gram-negative IM. Experimental IM X-ray form factor with WLBU2 taken and analyzed by Aria Salyapongse and Dr. Tristram-Nagle.

Figure 5.13 Chain order parameters for POPE and POPG with structured WLBU2-mod. The top panel shows the double-helix (d) and the bottom panel the single-helix (s) conformation. Simulation data were re-ordered to match NMR assumption of monotonically decreasing order parameters. Simulation data taken from equilibrated region of the all-atom IM simulated at 303 K. Experimental data collected via NMR at 310 K by Drs. Anja Penk and Daniel Huster.

LIST OF ABBREVIATIONS

AMP	Anti-Microbial Peptide
CD	Circular Dichroism
CPU	Computer Processing Unit
EDP	Electron Density Profile
FF	Form Factor
HMMM	Highly Mobile Membrane-Mimetic
IM	Inner Membrane
MD	Molecular Dynamics
NMR	Nuclear Magnetic Resonance
NPAT	Constant Normal Pressure, Lateral Area, and Temperature
NPT	Constant Normal Pressure and Temperature
PDB	Protein Data Bank
REST	Replica Exchange with Solute Tempering
RGY	Radius of Gyration
RMSD	Root Mean Square Deviation
TREM	Temperature Replica Exchange Method

CHAPTER 1: INTRODUCTION

1.1 Background of Antimicrobial Peptides

Antimicrobial peptides (AMPs) are a natural species of peptide found in all classes of life. In nature, these peptides are found to be the first line of defense in organisms and preemptively stop infections before causing serious harm.¹ AMPs are short-length proteins generally ranging from 12-50 amino acids; characteristically amphipathic, the peptide uses electrostatic interactions to create permeability in the cell membrane causing eventual flooding and cell necrosis.¹ Typically, AMPs belong to one of four classes: α -helical, β -sheet, extended, and a mixture of the other 3 types as shown in Figure 1.1. The most studied class of AMPs are cationic amphipathic antibacterial peptides, which will be the primary focus of this thesis.

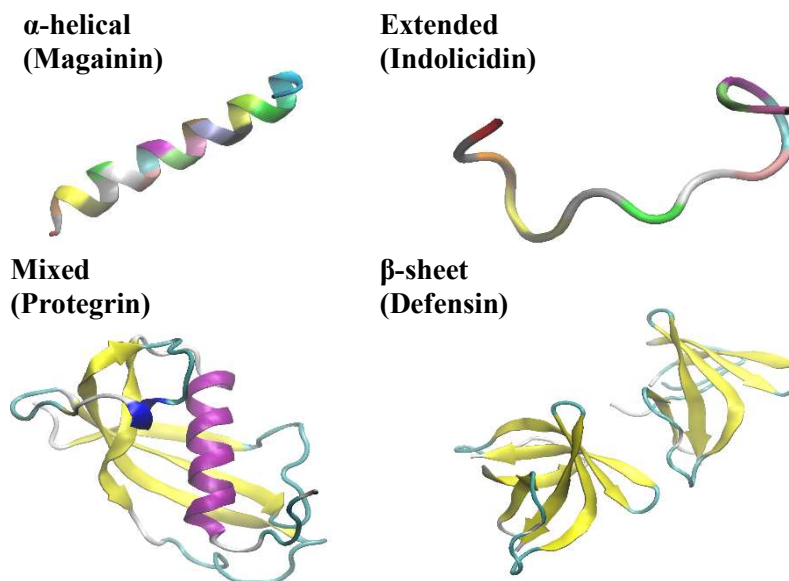


Figure 1.1 Four structural classes typically found of antimicrobial peptides: α -helical, extended, mixed, and β -sheet. Examples of each class are shown in parenthesis below.

The amphipathic nature of cationic α -helical AMPs is the key characteristic that provides function to the species. Electrostatic interactions are the driving force for the

known mechanisms of membrane attack that result in permeability and cell necrosis. Three understood mechanisms for this interaction have been illustrated in Figure 1.2; (a) Barrel-Stave Model, (b) Carpet Model, and (c) Toroidal Model.² Parallel placement of the peptide along the bilayer-water interface is shared among all three proposed models. The Barrel-Stave Model proposes an initial attraction between the positively charged portions of the AMP to the negatively charged polar head groups of the lipid bilayer. The hydrophobic portions then align with the lipid tails to create pores within the membrane allowing for water to flood the cell. In the Carpet Model, the AMPs attack by coating the membrane parallel to the interface and cause micelle-like chunks of lipids to come off the membrane allowing for water to flood the cell. The Toroidal Model is very similar to the Barrel-Stave Model; the only major difference being that the constructed pore walls along the water side of the interface are composed of hydrophilic lipid head groups and the hydrophilic portions of the AMP. Understanding the mechanism of AMP-membrane interactions will allow us to engineer synthetic peptides with improved selectivity and fitness, broadening our spectrum of antibacterial technologies.

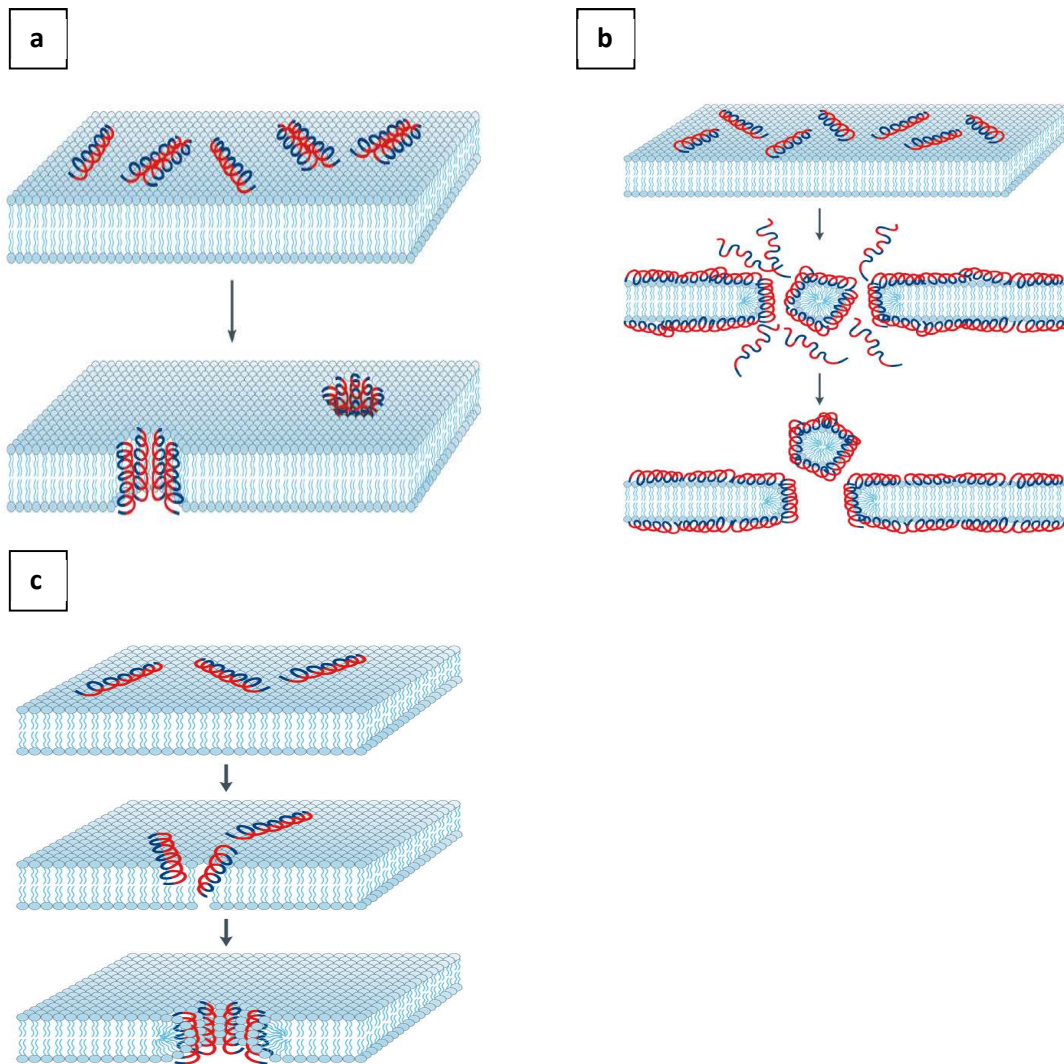
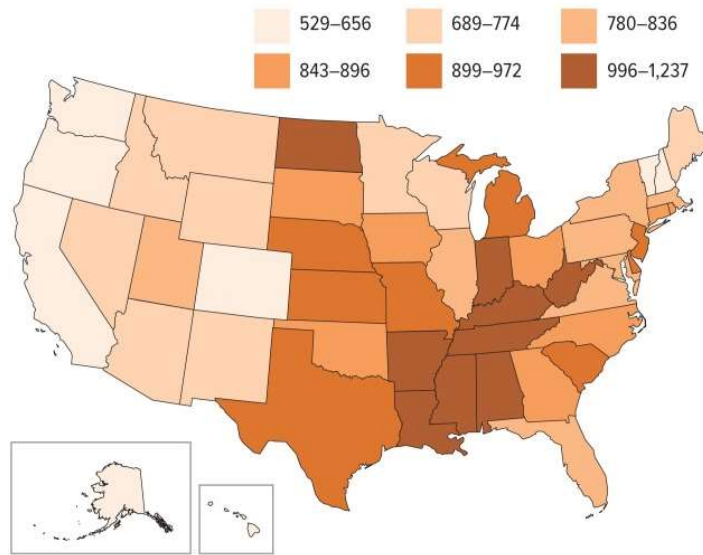


Figure 1.2 (a) Barrel-Stave Model showing perpendicular introduction of the AMP into the membrane forming water permeable pores within the membrane structure. (b) Carpet Model exhibiting parallel introduction of the AMP into the membrane forming micelle-like chunks of lipids causing the membrane structure to breakdown. (c) Toroidal Model with perpendicular introduction and mechanistic features like the Barrel-Stave Model, however the pores are composed of both the AMP and hydrophilic lipid head groups. Original figure 3,4,5 used with permission.²

1.2 New Antibiotic Methods Needed

Antibiotic technology has been one of the most important discoveries in medicine in the last century. Antibiotics provide cheap and effective immune system defense to all types of harmful bacteria. However, we currently have an antibiotic resistance crisis on our hands. As evolution dictates, strains of bacteria that have improved fitness become resistant

to existing antibiotic methods. However, due to the nature of bacteria, the evolutionary development timeline is unpredictable. The need for new antibiotics is always prevalent to continue protecting from these adapted resistant strains of bacteria since it is impossible to predict when we will see these strains develop. At the beginning, new antibiotic technologies were heavily researched and resistant strains were found less abundantly in nature. Over the years, due to widespread availability, antibiotics have been severely overused or misused resulting in increased resistant strains being discovered.³



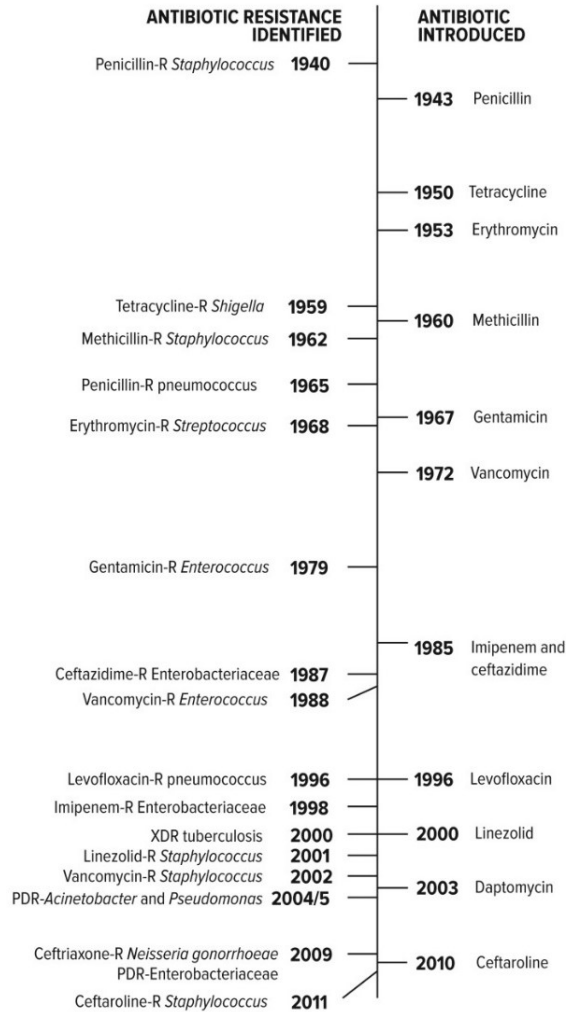
The frequency with which doctors prescribe antibiotics varies greatly from state to state. The reasons for this variation are being studied and might suggest areas where improvements in antibiotic prescribing (fewer unnecessary prescriptions) would be most helpful.

Figure 1.3 Antibiotic prescriptions in the United States for every 1,000 persons in 2010. Original figure 2 used with permission.³

Prescription use of antibiotics is not the only method of intake. Extensive overuse of antibiotics exists in the agricultural industry in both developed and developing countries worldwide. In the United States, an estimated 80% of all antibiotics are fed to animals to promote growth and prevent infections.³ The overuse of antibiotics in animals provide a

fertile breeding ground for resistant bacteria to develop while the non-resistant strains get killed off by the effective antibiotics. As well, the waste products of these antibiotic fed animals often contain a small percentage of antibiotics. The waste products get turned into fertilizer and runoff into ground water for crop production which provides another breeding ground for resistant bacteria to develop.³ The widespread overuse of antibiotics is heavily contributing to the resistance crisis we are facing today, however, the lack of new emerging methods is also a considerable factor.

For the last few decades, we have seen an impactful drop in the development of new antibiotic methods due to several factors; company mergers resulting in a lack of diverse research groups, economic and regulatory influences on research institutions, and a simple lack of interest because of more profitable opportunities available in other fields.³ It has been over five decades since the last new class of antibiotics specifically targeting gram-negative bacteria has been approved and only a handful of new antibiotics targeting gram-positive bacteria have been approved in that time.⁴ There has never been a more important time for significant advancement in the antibiotic field and antibacterial peptides could be the answer. There is plenty of motivation for antibacterial α -helical peptides as a substitute for current antibiotic therapeutics.



PDR = pan-drug-resistant; R = resistant; XDR = extensively drug-resistant
 Dates are based upon early reports of resistance in the literature.
 In the case of pan-drug-resistant *Acinetobacter* and *Pseudomonas*,
 the date is based upon reports of health care transmission or
 outbreaks. Note: penicillin was in limited use prior to widespread
 population usage in 1943.

Figure 1.4 A timeline detailing antibiotic development and introduction shown with known antibiotic resistant strains identified. Over the last two decades the number of developed antibiotics introduced has stayed regular while the number of antibiotic resistant strains of bacteria has substantially increased. Original figure 1 used with permission.³

CHAPTER 2: METHODS

2.1 Protein Structure Prediction Using the Robetta^{5,6} Server

Given the peptide sequence with unsolved structure, an initial starting structure is required for simulations for which the Robetta^{5,6} server was used. Robetta^{5,6} is an online protein prediction server developed by the Baker Laboratory at the University of Washington. Robetta^{5,6} uses the Ginzu prediction protocol to match protein chains into putative domains with reasonable confidence. The Ginzu protocol attempts to identify segments of the protein chain that align with protein data bank (PDB) templates wherever possible and if no alignment is made the protocol attempts to find units of the protein that could potentially fold into domains.^{5,6} The structure and 3-D models are constructed using homology modeling with comparisons made to proteins with solved structure and *ab initio* structure prediction methods designed by the Robetta^{5,6} server. Although Robetta^{5,6} uses advanced methods for protein structure prediction, it remains a challenge to predict with reasonable confidence structures of short-length proteins. Robetta^{5,6} has difficulty detecting homologs for comparative modeling in short sequences. The *de novo* modeling methods also are a challenge since a main component of Robetta's^{5,6} *de novo* modeling stems from the assumption that proteins typically form a soluble domain with a hydrophobic core. Short sequences often do not follow this trend which could potentially result in a bias in the energy calculations involved in the modeling and prediction protocol.^{5,6} As a result of such shortcomings, the Robetta^{5,6} server has a 28-residue minimum input length. Two valine residues were added to both the C-terminus and N-terminus of the 24-residue peptide WLBU2 (wildtype) and WLBU2-mod (slightly modified sequence, see the beginning of Chapter 3 for details) to meet the sequence length

requirements of Robetta^{5,6}. Valine was chosen as the additive residues to reduce steric and electrostatic effects. After Robetta^{5,6} outputted the potential initial structures, the additional valine residues were spliced out to recover the original 24-residue WLBU2 sequence. Robetta^{5,6} returned with confidence two distinct models for WLBU2. Since both models were predicted with confidence using the Robetta^{5,6} server, both were considered potential starting structures and further simulations were performed for both models.

2.2 WLBU2-mod Simulation Parameters

Three replicas of each system predicted by the Robetta^{5,6} server were built using the CHARMM-GUI *Quick MD Simulator* (Solution Builder)^{7,8} to study the structure of WLBU2-mod in an aqueous solvent. Both systems were constructed in a rectangular water box using the TIP3P⁹ water model. The termini of WLBU2-mod are both free termini (NH₂, COOH) and were simulated with terminal patching group NTER/CTER, which simulates the free termini, to match experimental setups as closely as possible. Brute-force molecular dynamics (MD) simulations of WLBU2-mod in an explicit aqueous solvent were built with CHARMM36 protein force field (C36)¹⁰ at 298.15 K with an NPT ensemble and carried out for 200 ns.

Following 200 ns of brute-force MD simulations of WLBU2-mod in water, the system showed no evidence of overcoming the high potential energy barriers. Enhanced sampling methods were required to uncover more information on the conformation and secondary structure of WLBU2-mod in an aqueous environment. We used replica exchange with solute tempering with an enhanced Hamiltonian acceptance protocol (REST2) that reduced the necessary computer processing units (CPUs) and allowed for more conformational space exploration.¹¹ REST2 for both systems were run with 24

replicas using C36m protein force field¹² with temperatures ranging from 300 K – 600 K within an explicit aqueous solvent. The force field was updated from C36 to C36m protein force field due to the latter's improved accuracy involving intrinsically disordered peptides.¹² Each trajectory included 500 cycles of exchange every 2 ps and the overall exchange rate was 30-40%. REST2 was performed for 150 ns to ensure convergence toward a common conformation amongst both the potential starting structures that the Robetta^{5,6} server predicted.

The motivation behind performing REST2 on both starting systems was to hopefully see both systems converge to a single common structure. In order to determine the most probable structure resulting from REST2, we utilized quantifiable metrics such as the radius of gyration (RGY), root mean square deviation (RMSD), ϕ and ψ backbone angles, and contacts between the residues. The radius of gyration is the root mean square distance of each atom to the center of mass of the entire protein. The radius of gyration indicates the compactness of the protein and can help define the secondary structure quantitatively throughout the simulation trajectory. CHARMM c41b2¹³ was used to calculate the RGY of WLBU2-mod after performing 150 ns of REST2.

After looking at the RGY, the next metric considered were the ϕ and ψ backbone angles. Residues existing in certain secondary structure conformations typically have specific ϕ and ψ backbone angles and looking at the entire peptide's ϕ and ψ angles on a Ramachandran plot can help determine overall secondary structure breakdown. Residues with torsion angles in the range $-180 < \phi < 0^\circ$, $-100 < \psi < 45^\circ$ are within the α -helical domain.¹⁴ Torsion angles in the range $-180 < \phi < -45^\circ$, $45 < \psi < 225^\circ$ are considered the β -sheet domain.¹⁴ Torsion angles within the range $0 < \phi < 180^\circ$, $-90 < \psi < 90^\circ$ are β -turns.¹⁴

The border region between the α -helix and β -sheet domains exist within the range $-160 < \phi < -65^\circ$, $45 < \psi < 90^\circ$.¹⁴ Using a TCL script via VMD¹⁵, we were able to determine the ϕ and ψ backbone angles for each residue throughout the entire trajectory of REST2.

The last quantifiable metric we used to help determine the most probable conformations was the number of contacts between residues. By determining the number of contacts and identifying where the contacts occur, we can identify possible points of electrostatic or hydrophobic interactions that play important roles in determining the structure and folding patterns of WLBU2-mod in an aqueous solvent. CHARMM c41b2¹³ was used to calculate the number of contacts. A minimum energy distance cutoff of 6.0 Å was used and only residues at least three apart in the sequence were considered eligible to be in contact.

2.3 Membrane Simulation Parameters

While studying the structure of WLBU2-mod in an explicit aqueous solvent environment via REST2, we were simultaneously performing MD on the bacterial IM mimic in an explicit aqueous solvent. Three replicas of an all-atom membrane were constructed using CHARMM-GUI's *Membrane Builder*^{7, 16-19} and simulated for 200 ns. A heterogenous lipid makeup with 50 lipids per leaflet composed of palmitoyloleoyl PE (POPE), palmitoyloleoyl PG (POPG), and 1,1',2,2'-tetraoctadecenoyl CL (TOCL2) in a 7:2:1 ratio respectively was constructed in a rectangular water box with a ratio of 30:1 water molecule to lipid. Neutralizing potassium atoms were added using the Monte-Carlo insertion method. The system was constructed using an NPT ensemble at 303.15 K and 1 bar with the C36 lipid force field²⁰. While WLBU2-mod was constructed with an NPAT ensemble, the membrane mimic was simulated with an NPT ensemble allowing the lipids

to flex with variable area while keeping the ratio of the unit cell in the x-y plane constant. The pressure was fixed at 1 bar using a Langevin piston. Equilibration of the membrane followed a six-step protocol using CHARMM¹³ and NAMD 2.9.

2.4 IM with Parallel Inserted WLBU2-mod Simulation Parameters

After simulating and studying both WLBU2-mod in an explicit aqueous solvent and the IM in an explicit aqueous solvent, the next step is to place WLBU2-mod above a Highly Mobile Membrane Mimetic (HMMM) lipid membrane. The motivation is to observe the interaction between the peptide and bilayer and to observe the structure of the peptide in the presence of the membrane. The peptide and membrane combined system was constructed using CHARMM-GUI's *HMMM Builder*^{7, 21} using a PDB file created from the most probable conformations of WLBU2-mod after analysis of REST2 simulations. Three replicas of four conformations, two of each system outputted from Robetta^{5, 6}, were chosen for simulation with the HMMM membrane build for a total of 12 MD simulations. HMMM setup with an acyl carbon number of 6 cleaves the acyl chain beyond the 6th carbon and replaces the tails with dichloroethane (DCLE). This allows for increased flexibility for the membrane as the bilayer center is essentially a liquid solution. Using a HMMM build can act as a speed buffer that can offer 10x speed up to a normal all-atom build for MD simulations.²² The peptide was positioned along the x-y plane for parallel insertion and placed at least 10 Å away from the top leaflet. Additional water molecules were added to ensure the peptide remained within the rectangular water box. Each replica inserted the peptide with a 5° tilt away from the x-y plane relative to the previous replica (replica 1 inserted 0° off the x-y plane, replica 2 inserted 5° off the x-y plane, replica 3 inserted 10° off the x-y plane) to avoid biased binding events. A lipid area

scaling factor of 1.2 was used to have reduced lipid packing and faster lipid motions. The combined systems were constructed using an NPAT ensemble at 310.15 K using C36 lipid force field²⁰ and C36m protein force field¹². The pressure was held constant at 1 bar with a Langevin piston. MD was performed on all systems for 200 ns to ensure equilibration. Afterwards, the binding mechanisms of the peptide and HMMM systems were observed, and dissimilar binding interactions were chosen for conversion to all-atom systems. Three of the original 12 peptide and HMMM systems were chosen for conversion to an all-atom system and MD was performed for an additional 150 ns. During the conversion, the ensemble was changed to an NPT ensemble. By removing the area constraints, we allow the system to naturally expand and contract in response to the protein.

The 12 combined systems constructed previously used peptide conformations resulting from REST2. These peptides were unstructured after overcoming the surface potential energy barriers. We decided to additionally observe the effects of structured helical WLBU2-mod with the IM. Three replicas of each of the starting structures outputted using Robetta^{5, 6} (six systems total) were inserted into a HMMM build of the IM and MD was performed for 150 ns. Each system was built using the same parameters as the unstructured HMMM combined systems detailed above. The binding motifs and penetration distance were observed, and one system of each structure was converted to an all-atom system. MD was performed for an additional 150 ns using an NPT ensemble to allow the lipids to naturally expand and contract in response to the protein. The results and discussions of all simulations are detailed in the following chapters.

CHAPTER 3: WLBU2-MOD PEPTIDE IN EXPLICIT AQUEOUS SOLUTION

3.1 WLBU2-mod Background and Robetta^{5,6} Protein Structure Prediction

This thesis will focus on the computational analysis of simulating WLBU2-mod in an explicit aqueous solvent as well with the gram-negative bacterial IM. The work presented here was done in collaboration with two other groups. Dr. Tristram-Nagle's lab at Carnegie Mellon University gathered the experimental data including the X-ray scattering and circular dichroism (CD) measurements to which our computational results will be compared. Simulation of the outer membrane was performed by Dr. JC Gumbart's group at Georgia Tech in collaboration with Dr. Tristram-Nagle's lab.

WLBU2 (RRWVRRVRRWVRRVVRVRRWVRR) is a 24-residue cationic amphipathic peptide consisting of 13 Arg residues, 8 Val residues, and 3 Trp residues. Our goal is to observe the structure of WLBU2 in the presence of the gram-negative bacterial IM and observe the interaction between the antibacterial peptide and lipid bilayer. The first step toward achieving our goals is to solve the structure of our peptide sequence. We used the Robetta^{5,6} server which uses an intelligent comparative structure matching protocol as well as *de novo* modeling methods to predict the structure of a given protein sequence.

Unfortunately, at the beginning of the project there was an error made when attempting to solve the structure of the peptide. When entering the sequence into the Robetta^{5,6} server for structure prediction, the sequence was inputted incorrectly with the following sequence (RRWVRRVRRVWRRVVRVRRWVRR). The middle two Val and Trp residues (underlined) were adjacently swapped and the structures outputted were based off this incorrect sequence. Unfortunately, this mistake was not caught until after the project was nearly complete. It is paramount to clarify that the analyses performed and

discussed in this thesis are all based on the modified sequence while experimental data used for comparison maintains the original wild-type sequence. To keep things consistent, when referring to the peptide with the modified sequence WLBU2-mod will be used to identify this peptide while WLBU2 will refer to the wild-type. Afterwards, in deciding whether this sequence modification was significant enough to merit the reproduction of all simulations and analyses, the wild-type sequence was inputted into the Robetta^{5, 6} server and the solved structure was compared to the modified sequence structure outputted. As before, Robetta^{5, 6} predicted both a double-helix and single-helix model as two potential starting conformations. Looking at Figure 3.1, the wild-type and modified sequence structures are consistent for both the double-helix and single-helix structures. After aligning WLBU2 and WLBU2-mod, we found the root mean square deviation (RMSD) values of WLBU2 using WLBU2-mod as the reference state. The RMSD gives us the average distance between the backbone atoms of the two structures after superimposition. Small RMSD values tell us the two superimposed molecules are similar in structure. The double-helix structure had a weighted average RMSD value of 1.624 Å and the single-helix structure had a weighted average RMSD value of 0.164 Å. Relative to dissimilar conformations, these values tell us that the structures are in fact extremely similar. It was concluded that the residue swap mistake had an insignificant change in the overall structure and characteristics of the peptide and that the results of simulations performed using WLBU2-mod would be viable for experimental comparisons.

Robetta^{5, 6} returned two distinct structures for WLBU2-mod. The first structure depicts a single straight α -helix (single-helix), as shown in Figure 3.1a. The second

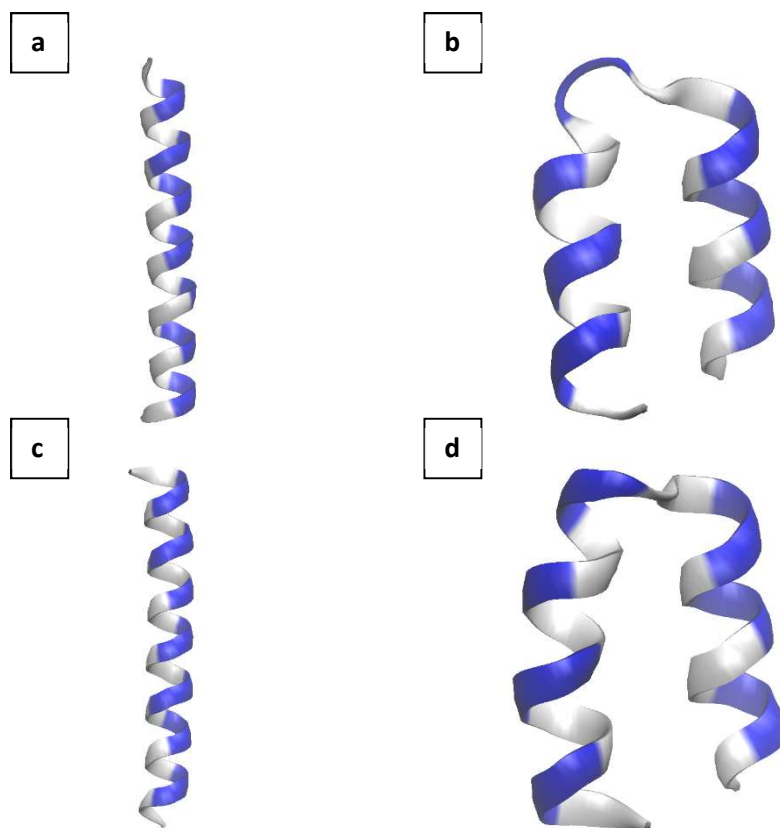


Figure 3.1 (a) Straight α -helix WLBU2 (b) α -helix bent WLBU2 (c) Straight α -helix WLBU2-mod (d) α -helix bent WLBU2-mod. WLBU2 is composed of 13 Arg, 8 Val, and 3 Trp. Colored by residue type; non-polar (white) and polar (blue).

predicted structure is an α -helix bent in the middle forming two helices (double-helix), as shown in Figure 3.1b.

Both Robetta^{5, 6} predicted structures exhibit physical separation between hydrophobic Val and Trp and hydrophilic Arg which are prominent characteristic features of cationic AMPs. Both structures were outputted from Robetta^{5, 6} with confidence, therefore, neither potential structure could be eliminated and both predicted structures were carried out for further analysis.

3.2 Brute-Force Molecular Dynamics

Both the single-helix and double-helix predicted initial structures were inputted into CHARMM-GUI's *Quick MD Simulator* (Solution Builder)^{7, 8} where the peptide was

inserted into an explicit aqueous solvent. Brute force MD was performed on three replicas of each single-helix and double-helix system (six systems total) for 200 ns. However, after 200 ns of brute-force MD, none of the six systems showed any ability to overcome the high surface potential energy barrier.

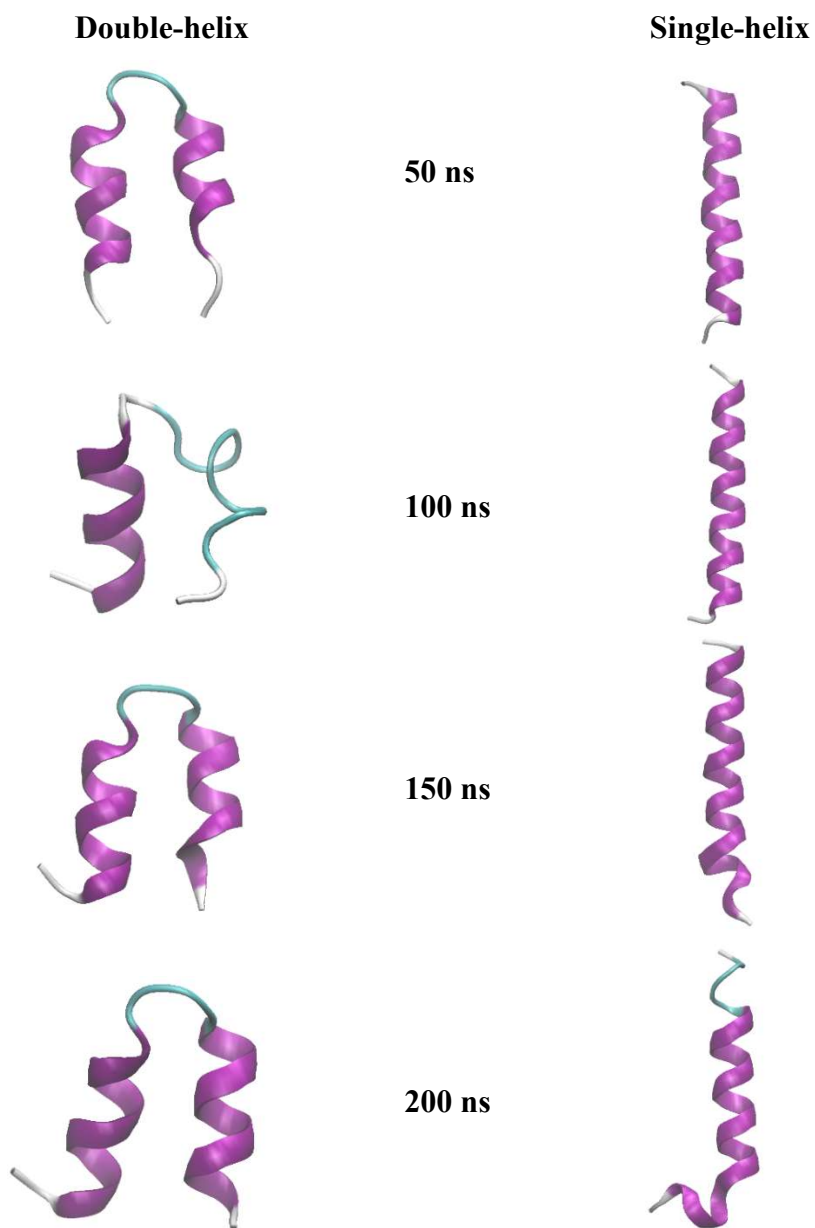


Figure 3.2 Brute force MD full trajectory time series after 200 ns for both double-helix and single-helix systems.

Comparing the starting structures to the structures after 200 ns of brute force MD, both systems maintained nearly all its original secondary structure. Figure 3.2 displays some loss of α -helical character in the double-helix system at 100 ns. However, the α -helical character is immediately recovered and kept throughout the remaining trajectory. The loss of secondary structure is credited to being on the edge of the equilibrated space and therefore not indicative of the equilibrated regime. From the results of brute force MD, it was apparent that traditional MD methods would not suffice in overcoming the energy barriers in WLBU2-mod with the short timescales simulated to be able to accurately sample protein structure.

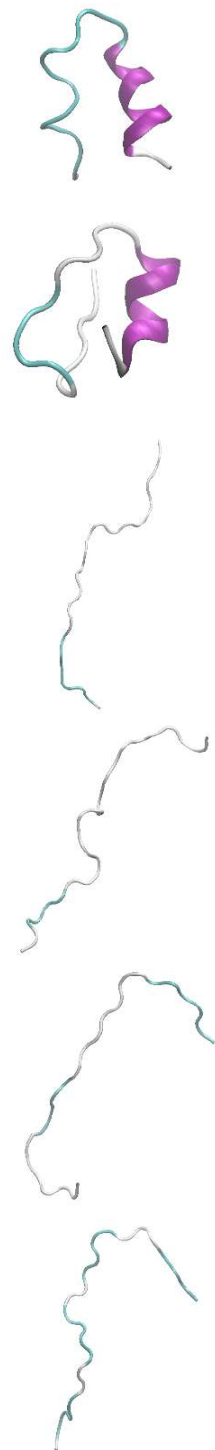
3.3 Replica Exchange with Solute Tempering (REST2)

Following brute-force MD simulations of WLBU2-mod in water, enhanced sampling methods were required to uncover more information on the conformation of WLBU2-mod in an aqueous environment. To overcome the high surface energy barriers of WLBU2-mod and explore more conformational space beyond traditional brute force MD, we used replica exchange with solute tempering (REST2) with an enhanced Hamiltonian protocol that reduces the CPUs required compared to typical replica exchange with solute tempering (REST1) or temperature replica exchange method (TREM).¹¹ REST2 overcomes TREM's shortcomings of poor scaling with system size and has modified the Hamiltonian acceptance protocol to be independent of the number of explicit water molecules in the system.¹¹ This change in the acceptance protocol reduces the CPUs required for REST2 to explore the same amount of conformational space as REST1. Traditional brute-force MD simulated at low temperatures or short timescales typically cannot get over high energy barriers and tends to get stuck in local energy minima

conformations. REST2 bypasses the pitfalls of traditional MD and can help overcome high surface energy barriers allowing for the exploration of more conformational space at lower temperatures and shorter timescales. The tradeoff for REST2 is the amount of parallel processing power required to run energy calculations for all replicas simultaneously. In consequence, REST2 was only performed on one replica of each single-helix and double-helix system.

The full 150 ns trajectory is shown in Figure 3.3 which details the denaturing progress of both systems as a result of REST2. Whereas in 200 ns of brute-force MD WLBU2-mod showed barely any ability to denature, within 25 ns of REST2 both systems have partially or completely unraveled toward an equilibrated structure. Immediately, the effects of REST2 as an enhanced method of MD are observed. By swapping conformations with replica systems at higher temperatures, even the lower temperature system can easily overcome high surface energy barriers and break-out of local minima traps. As the timescale increases, the peptides seem to denature into a random extended structure with no noticeable secondary structure. The goal of REST2 was to hopefully observe the peptides starting from both the single-helix conformation and double-helix conformation conform to a single equilibrated structure. In order to confirm if REST2 resulted in a uniform structure, detailed quantifiable analytics on the structure of WLBU2-mod are needed beyond observation of the 3-D modeled structure.

Double-helix



Single-helix

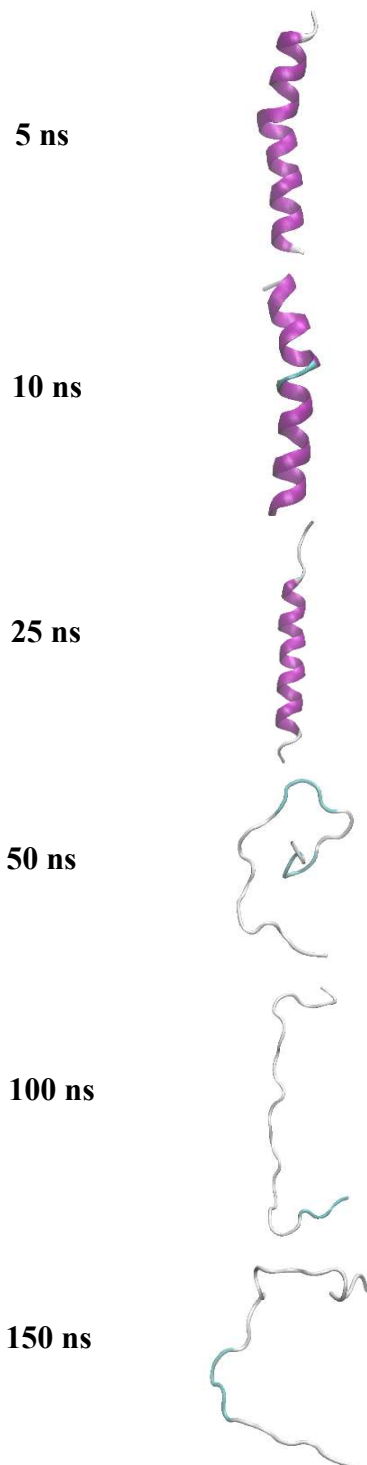


Figure 3.3 REST2 full trajectory time series after 150 ns for both double-helix and single-helix systems.

3.4 WLBU2-mod Analysis

The motivation behind performing MD and REST2 on WLBU2-mod in an explicit aqueous solvent is to observe the structure of WLBU2-mod in the presence of water solvent and to uncover potential conformations that are most probable for interacting with a mimic of the gram-negative bacterial IM. Figure 3.3 shows the 3-D model of WLBU2-mod starting from both single-helix and double-helix conformations. Observing the structure through images and movies gives general information on the denaturing of the peptide, however, without detailed analytics on the structure these images are useless in helping determine a uniform conformation for simulation with IM.

Multiple protein analytical metrics were considered in deriving the most probable conformations resulting from REST2: radius of gyration (RGY), root mean square deviation (RMSD), ϕ and ψ backbone angles, and residue contacts. The RGY helps defines how compact the peptide is in 3-D space by measuring the average distance of the termini to the center of mass of the molecule. The RMSD measures the average distance of the atoms between two superimposed structures. For this analysis, the reference state used for comparison was the structure outputted last from MD simulations. The backbone ϕ and ψ angles can help identify possible secondary structure motifs present. Using these protein analytical tools as quantitative metrics help define a set of characteristics that determine highly probable starting structures for further simulation. The appearance of structure convergence in the 2-D contour plots shown in Figure 3.4 suggests the equilibrated region for both single-helix and double-helix systems converges within the time block 75-100 ns.

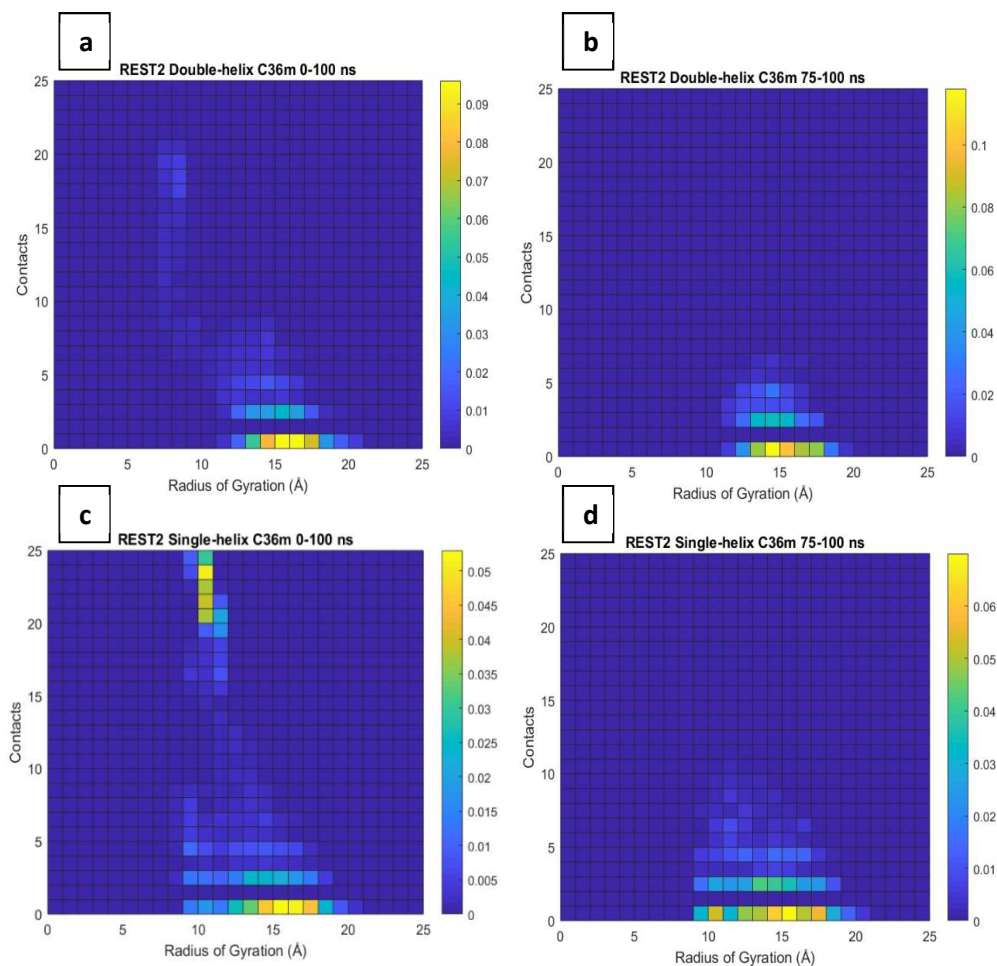


Figure 3.4 2-D contour plot for the RGY and number of residue contacts for (a) 0-100 ns of REST2 for double-helix system (b) 75-100 ns of REST2 for double-helix system (c) 0-100 ns of REST2 for single-helix system and (d) 75-100 ns of REST2 for single-helix system.

Looking at Figure 3.4 (a) and (c) both the single-helix and double-helix full trajectory densities shown in the color bar to the right are lower than that of the equilibrated region (b) and (d) and the data is spread out considerably more. After considering the equilibrated region of REST2 to be 75-100 ns and finding the RGY value of each structure's state within this block, we determined that the RGY equilibrates within the range of $17 \text{ \AA} \pm 3 \text{ \AA}$ for the single-helix system and $16 \text{ \AA} \pm 3 \text{ \AA}$ for the double-helix system.

The other metric considered in Figure 3.4 are the number of residues in contact with one another. This analysis only considered residues at least three residues apart along the backbone sequence to be eligible for contact. The motivation was to determine if the peptide began to conform to a certain conformation based on some steric or electrostatic forces present. Figure 3.4 demonstrates that for both the single-helix and double-helix systems two conformations typically existed at any given time. Either the peptide had no residues in contact with one another or at most two residues were in contact. Evident by the 2-D contour densities within the equilibrated time block, the probability of either peptide having 2 contacts is less than the probability of having 0 contacts. Table 3.1 demonstrates that although the more probable conformation exhibits no residue interplay, there exists a significant portion of the equilibrated trajectory where contacts are observed. This was a major factor when deciding which structures to proceed with and ultimately both conformations were considered.

The last metric considered, and ultimately the most important analytic for determining the equilibrated structure characteristics, are the ϕ and ψ backbone angles. We defined regions of these backbone angles in Chapter 2 that allowed us to determine the overall secondary structure based on percentages of residues that had ϕ and ψ backbone angles within these defined regions. The Ramachandran plots for REST2 of both systems, broken up into time blocks of 25 ns, quantify the change in secondary structure over time. Both systems started with greater than 50% α -helical structure and equilibrated toward a structure containing 20-25% α -helical structure. The loss of α -helical structure as a result of REST2 indicates the disordered peptide favors a random coil structure. The high surface energy barriers that brute force MD failed to overcome are likely attributed to the large

percentage of α -helical structure in the starting conformations. Using a more rigorous conformational exploration tactic allowed us to breakdown the peptide and explore a disordered regime containing roughly $\sim 20\%$ α -helical.

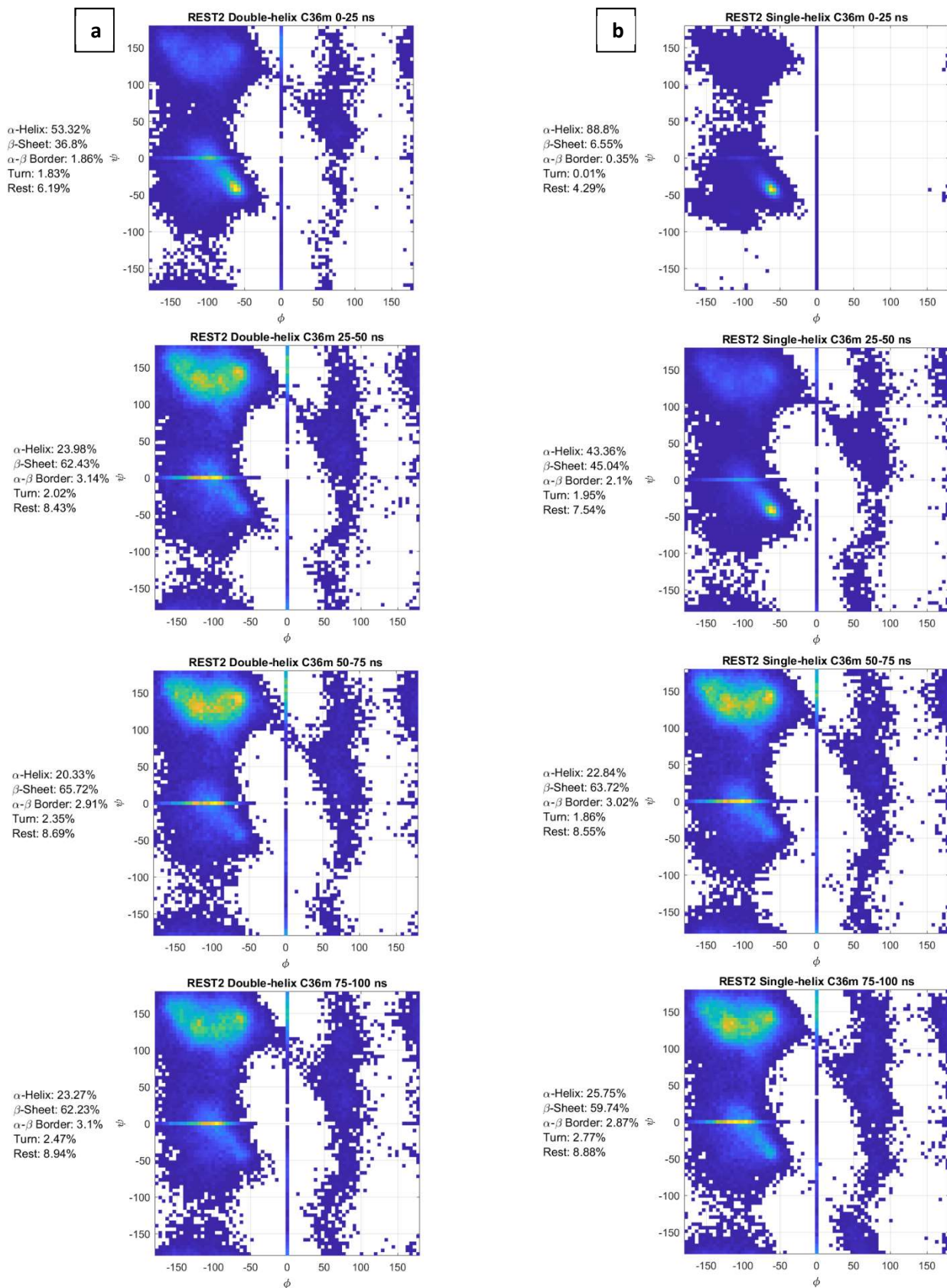


Figure 3.5 Ramachandran plots for REST2 for (a) double-helix (b) single-helix.

Table 3.1 presents the culmination of the quantitative analysis performed on the REST2 simulations for both the single-helix and double-helix systems. Four distinct structures were chosen based on their probability to occur within the equilibrated trajectory given the most probable parameters. The first structure chosen derived from the single-helix trajectory consisted of zero residue contacts, five α -helical residues (20%), 16 β -sheet residues (66%), and an RGY of 17 Å. The structure with these exact parameters, with an RGY flexibility of 3 Å, occurred 31.5% of the entire equilibrated region of the REST2 simulation for the single-helix system. The second structure derived again from the single-helix starting system, exhibited nearly the same characteristics as the first structure except with a residue contact between V14 and W11, occurred for 19.0% of the equilibrated region. Although the probability to exist is less than the first structure derived from the single-helix system, this still made up a significant portion of the equilibrated region and structures with contacts could not be eliminated for further analysis. The other two structures were chosen using the same metrics but derived from the double-helix starting system. Our initial goal for performing brute-force MD and REST2 was to find a converged denatured structure for WLBU2-mod in an explicit aqueous solvent; based on Table 3.1, there is evidence for convergence of a common unstructured peptide conformation amongst both the single-helix and double-helix REST2 simulations. Based on the results of the quantitative analysis, WLBU2-mod in aqueous solvent exhibits ~20% α -helical character, ~70% β -sheet character, and little to no residue interplay.

Table 3.1 Four structures chosen for simulation with gram-negative bacterial IM mimic based on percent occurrence within equilibrated region resulting from REST2.

	Starting Structure	Residue Contacts	α-Residues	β-Residues	RGY	% Occurrence
1	Single-helix	0	5	16	17 Å \pm 3 Å	31.5%
2	Single-helix	2	4	17	17 Å \pm 3 Å	19.0%
3	Double-helix	0	4	17	16 Å \pm 3 Å	50.0%
4	Double-helix	2	4	17	16 Å \pm 3 Å	23.1%

In a joint effort to determine the correct conformation of the peptide, Aria Salyapongse took CD measurements and helped analyze the results along with Dr. Tristram-Nagle to determine the expected secondary structure of WLBU2. CD is an absorption spectroscopy experiment that measures circularly polarized light to optically investigate the structure of proteins. Similar to the Ramachandran plot where secondary structures have typical backbone angles, secondary structures also give off typical polarized light that can be measured using CD spectroscopy. By comparing the experimental results to the typical motifs, we can determine the breakdown of the secondary structure of WLBU2. CD data for WLBU2 taken at neutral pH and 310 K found WLBU2 to exist in a water solvent with primarily random coil secondary structure with significant β -sheet character. Figure 3.6 shows the results of the CD experiments for 13 μ M WLBU2 in water and Table 3.2 details the secondary structure breakdown of the peptide analyzed using the Brahms and Brahms data set.²³ Experiments suggest WLBU2 exists in water in a conformation consisting mainly of random coil and β -sheet without much presence of α -helical secondary structure. Robetta^{5, 6} predicted structures, both single-helix and double-helix, have both $> 70\%$ α -helical character. After REST2, WLBU2-mod in water loses most of the original α -helical structure and moves toward a

random coil regime. This conformation is similar to the secondary structure for WLBU2 in water found experimentally using CD.

Table 3.2 Secondary structure breakdown of WLBU2 in water, pH 7.0, 310 K.

Concentration	α -helix %	β -sheet %	β -turn %	Random %	R ²
13 μ M	3	35.5	2.5	59	0.99

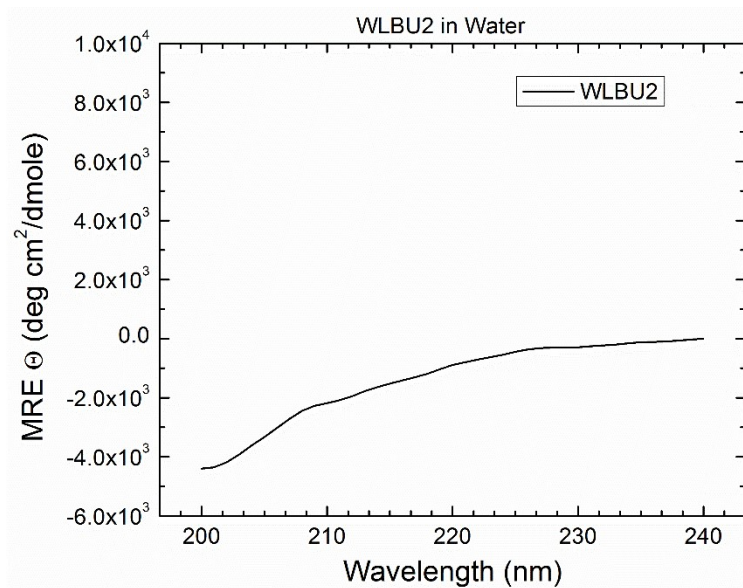


Figure 3.6 Experimental CD of 13 μ M WLBU2 in water. The difference between left and right circular polarized light is measured as the molar ellipticity and plotted against the wavelength of absorption. CD taken by Aria Salyapongse and analyzed by Aria Salyapongse and Dr. Tristram-Nagle.

CHAPTER 4: INNER MEMBRANE MIMIC OF GRAM-NEGATIVE BACTERIA

4.1 Membrane Composition

The premier focus of this thesis is simulating and analyzing the interactions between WLBU2-mod and the gram-negative bacterial IM. The real *E. coli* IM is composed of ~25 different complex lipids but can be simplified by the main headgroup components. Predominantly, zwitterionic PE makes up about 75% of the inner membrane composition with the rest composed of anionic PG and CL.²⁴ Simplistic mimics have typically forgone CL and opted to simulate with just PE and PG in a 3:1 ratio.²⁵ However, the inclusion of anionic CL allows for a more realistic mimic of the IM by including a four-tailed lipid type in contrast to the predominant two-tailed PE and PG. The IM mimic chosen for our simulations consists of 50 lipids per leaflet composed of palmitoyloleoyl PE (POPE) (16:0,18:1), palmitoyloleoyl PG (POPG) (16:0,18:1), and 1,1',2,2'-tetraoctadecenoyl CL (TOCL2) (18:1,18:1) in a 7:2:1 ratio of POPE:POPG:TOCL2 (see Figure 4.1 for the chemical structure of these lipids). TOCL can exist in two forms, either 1^- or 2^- charge based on the phosphate head groups protonation level and environmental conditions. At ambient conditions and neutral pH, the phosphate head groups of TOCL is taken to be completely deprotonated resulting in 2^- charge.²⁶

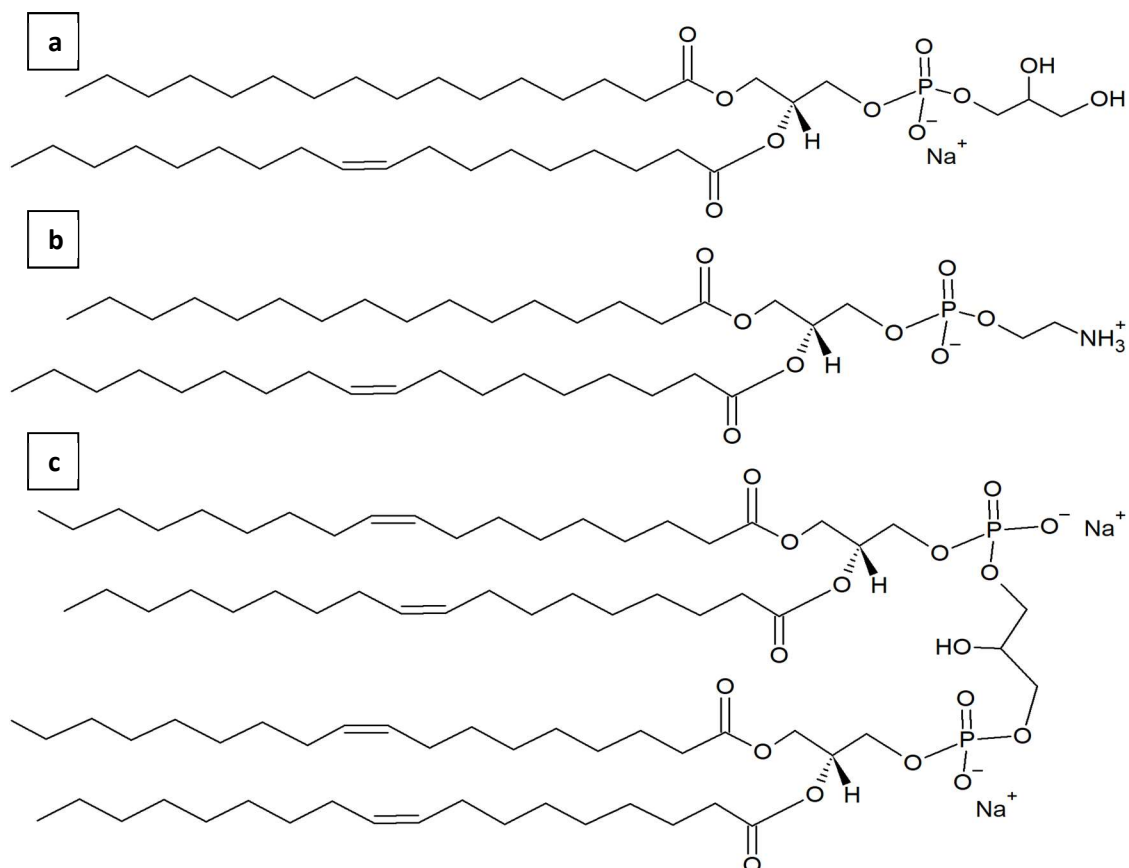


Figure 4.1 (a) palmitoyl-oleoyl PE (POPE) (16:0,18:1) (b) palmitoyl-oleoyl PG (POPG) (16:0,18:1) (c) 1,1',2,2'-tetraoctadecenoyl CL (TOCL2) (18:1,18:1).

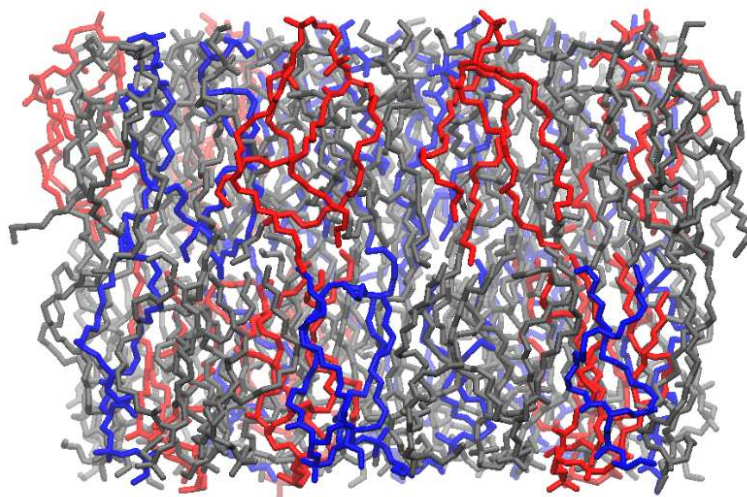


Figure 4.2 Gram-negative bacterial IM mimic consists of 50 lipids per leaflet composed of POPE (gray), POPG (blue), and TOCL2 (red) in a 7:2:1 ratio.

4.2 Results of IM in Aqueous Solvent MD Simulations

MD simulations for the three all-atom IM mimic replicas were performed for 200 ns until complete equilibration (Figure 4.2 shows a snapshot view of this membrane). To determine complete equilibration of the membrane, we observed the surface area per lipid over the entire trajectory. Figure 4.3 shows the observed plots for SA/lipid over the 200 ns of MD simulations for the three all-atom IM replicas. Considering the last 100 ns to be the equilibrated region, the replicas each had an average SA/lipid of $66.7 \pm 0.2 \text{ \AA}^2$, $66.5 \pm 0.2 \text{ \AA}^2$, $65.8 \pm 0.2 \text{ \AA}^2$, respectively. Combining the averages and standard errors gives an overall SA/lipid weighted average of $66.3 \pm 0.2 \text{ \AA}^2$.

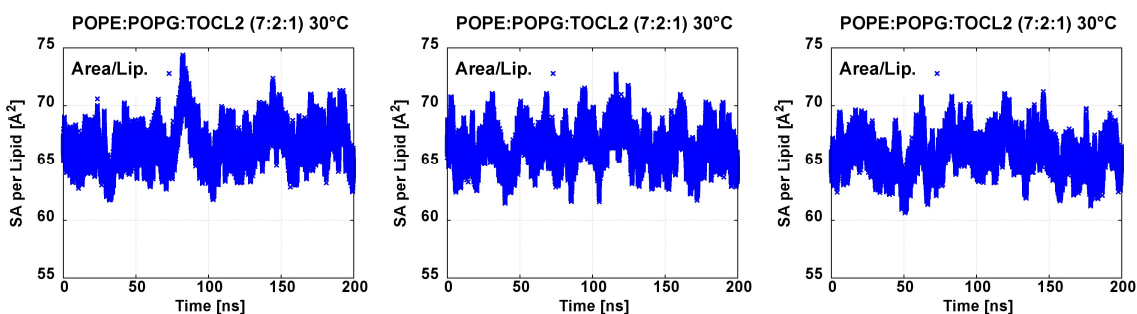


Figure 4.3 Surface area per lipid for 200 ns of brute force MD for the three all-atom IM replicas.

After determining the equilibrated region to be taken as the last 100 ns of MD simulations for all three replicas, we wanted more insight into the atomistic detail of the molecular simulations involving the IM in an explicit aqueous solvent. Order parameters can help define on an atomistic level the flexibility of the lipids. Order parameters take in consideration the angles between the backbone hydrogens and relative carbons to calculate the order for that carbon index. By using the bond angles of the backbone, the order parameters can be directly correlated with backbone flexibility. Flexible lipids can be sensitive to fluctuations in the structural orientation when in the presence of small

molecules and thus makes chain order parameters an important quantifiable metric to consider.

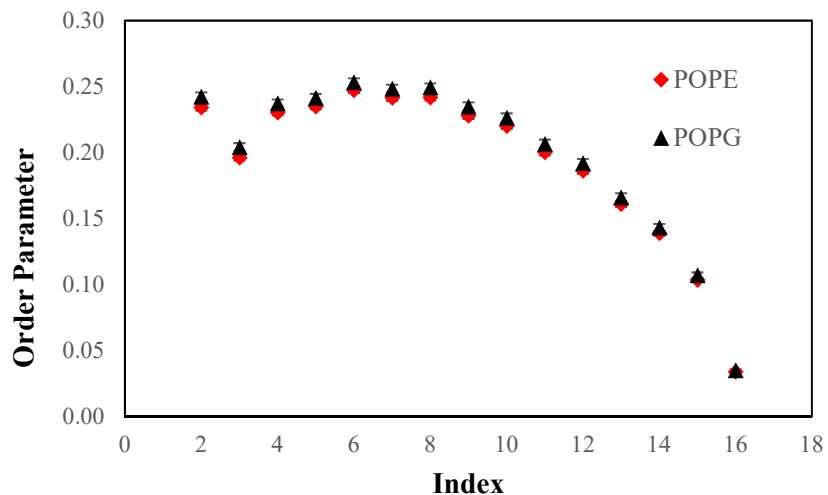


Figure 4.4 Chain order parameters for the sn-2 chain for POPE and POPG taken from the equilibrated region of the three all-atom IM replicas. Data taken as an average from the three replicas with the standard deviation shown as vertical error bars.

Near the headgroup we see fluctuating order. As we move down the backbone toward the bilayer center, we see decreasing order as expected for fully saturated chains. Considering the structural similarities between POPE and POPG lipids, it is expected that there is very little difference in the order between the two. Without any peptide present, the order profile is as expected.

Our collaborative experimenters used ^2H nuclear magnetic resonance (NMR) spectroscopy with deuterated lipid acyl chains to determine the order parameters of POPE and POPG. Deuterated NMR is a powerful technique for measuring the order of the hydrophobic core of membranes as it replaces protons with deuterons that have a spin of 1 compared to $\frac{1}{2}$ for protons. In order to compare with experimental NMR data collected by Drs. Anja Penk and Daniel Huster (Universität Leipzig in collaboration with Dr. Tristram-Nagle's lab), the order parameters were re-ordered to coincide with the monotonically decreasing NMR assumption. Even though we see in our simulation results that the highest

order persists around the C6-C8 range, NMR assumes the highest order carbon to be C2 with monotonically decreasing order down the backbone. Comparing our simulation results to the NMR results, we see similar order for the higher-order positions but then a divergence in agreement toward the mid-level order positions. Both the experiment and simulation suggest similar order for both POPE and POPG, but the experimental results observe decreased order for both lipids compared to our MD simulations. This disagreement can be explained when taking into consideration the different temperatures for the data collection. NMR experiments were conducted at 310 K while MD simulations were performed at 303 K. A higher temperature will cause increased lipid motion and chain isomerization, resulting in decreased order.

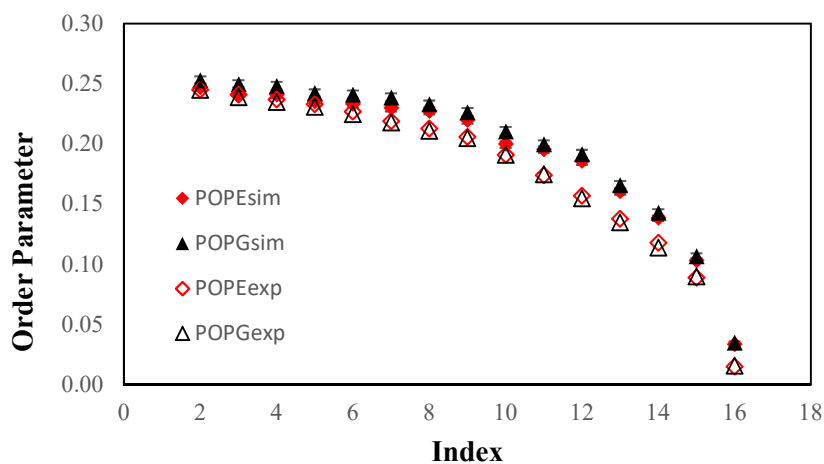


Figure 4.5 Chain order parameters for control POPE and POPG. Simulation data were re-ordered to match NMR assumption of monotonically decreasing order parameters. Simulation data taken from equilibrated region of the three all-atom IM replicas simulated at 303 K. Experimental data collected via NMR at 310 K by Drs. Anja Penk and Daniel Huster.

Another metric used for comparing the experimental control results to our simulation results utilizes the X-ray form factors (FF) collected and analyzed by Aria Salyapongse and Dr. Tristram-Nagle. The y-axis is measured in $e/\text{\AA}^2$ and is essentially the

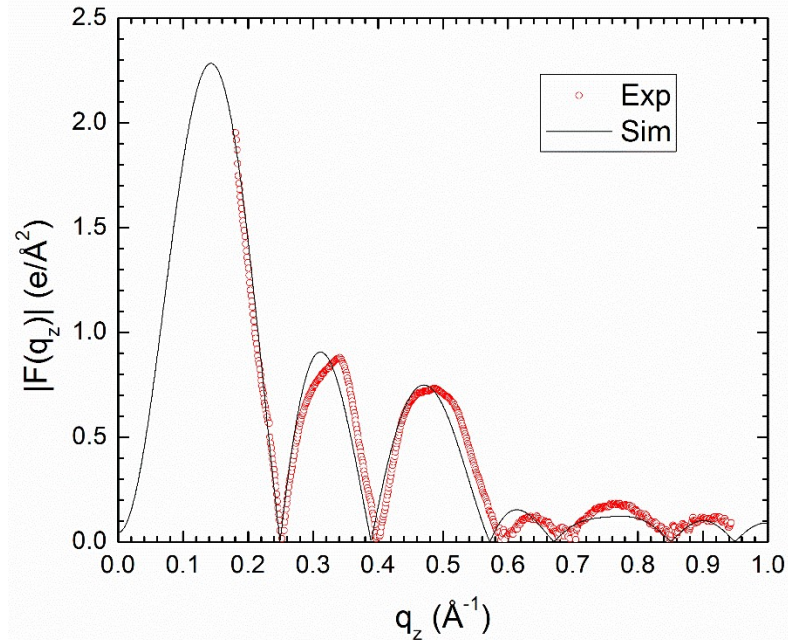


Figure 4.6 X-ray form factors for the gram-negative IM POPE:POPG:TOCL2 (7:2:1) control system without the peptide. Experimental results collected and analyzed by Aria Salyapongse and Dr. Tristram-Nagle at 310K. Simulations results collected using the equilibrated region of the IM MD simulations.

square root of the intensity collected using X-rays. The data is put through the Fourier transform and using model fitting the curves shown are outputted. The control FF shows good agreement between the experiment and simulation, where accurate crossing points ($F(q_z)=0$) indicates accurate surface area per lipid. The control FF will help establish a baseline for comparing the IM when we introduce the peptide in Chapter 5.

One of the most common analyses conducted for lipid bilayers is the electron density profile (EDP). The EDP tells us information on the location of specific atom groups within the membrane. We have found the EDP for the IM in an explicit aqueous solvent, which can be seen in Figure 4.7. For this profile some groups were left out to highlight the important groups of interest. We observed a typical density profile for the IM without the peptide in which the water and phosphate headgroups primarily make up the entire density at the interface. Toward the center of the bilayer the density is composed of the methylene

and methyl atoms of the non-polar backbone tail. The unsaturated C9-C10 carbon atoms can also be found in between the headgroups and methyl carbon densities as expected. The density profile was taken from the equilibrated region of the last 100 ns of MD simulation. The IM maintains its structural integrity throughout the entire equilibrated region for all three replicas.

Table 4.1 Thickness data from equilibrated region of three all-atom control IM systems. Values reported as averages with standard error between the three replicas.

Combined	
D_{HH}	41.0 ± 0.5 Å
D_B	39.9 ± 0.3 Å
2D_C	30.8 ± 0.2 Å

Table 4.1 gives the calculated thickness data for the three all-atom IM systems. The data were collected using the last 100 ns of MD simulation as the equilibrated region. D_{HH} is the headgroup to headgroup distance for the bilayer. This is calculated by measuring the distance between the two peaks of the densities from the upper-leaflet to the lower-leaflet. D_B is the overall bilayer thickness which is like the D_{HH} but is calculated measuring the distance between the midpoints of the water profile. It is assumed that the midpoint of the water density can be used to signify the beginning and end of the bilayer even though this is slightly less than the D_{HH} which takes into consideration only the peak density values. D_C is the hydrophobic thickness which is calculated by measuring the distance between the midpoints of the acyl chains in the density profile. Since we use the midpoints of the acyl chains, to calculate the overall hydrophobic thickness we need to double the D_C thickness. Table 4.1 reports the value $2D_C$ for the total hydrophobic thickness.

Following MD simulations of the IM and REST2 analysis on the peptide, the next step is to combine the systems and observe the interaction between the peptide and IM.

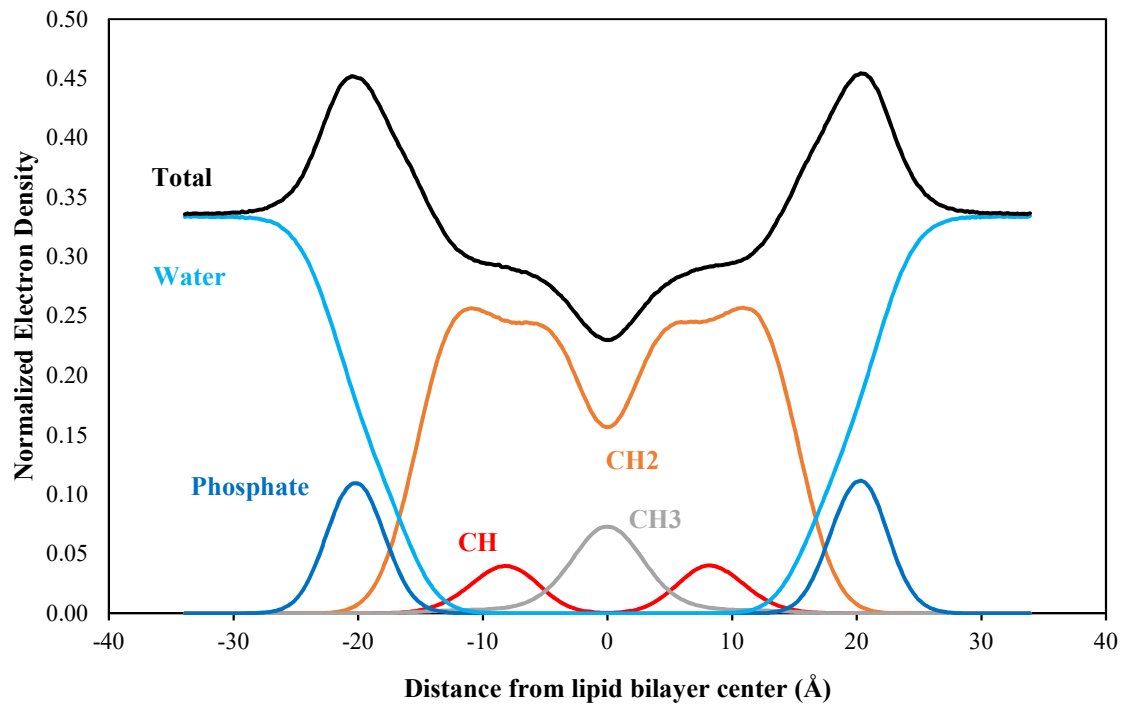


Figure 4.7 Electron density profile (EDP) for the bacterial IM in an explicit aqueous solvent.

CHAPTER 5: WLBU2-MOD PARALLEL INTRODUCTION WITH INNER MEMBRANE MIMIC

5.1 Results of Unstructured WLBU2-mod and IM

Using the four most probable conformations of the peptide resulting from the REST2 analyses, 12 systems were constructed with a HMMM build of the IM mimic. These systems were run for 200 ns and then the binding motifs were observed. Of the 12 systems, three were chosen for conversion to an all-atom lipid system and run for an additional 150 ns without area constraints. Figure 5.1 shows the initial WLBU2-mod placement for the three HMMM systems chosen for all-atom conversion as well as the final binding state before conversion to an all-atom system. All three systems showed peptide binding within the first few nanoseconds. The motivation to use a HMMM build before converting to an all-atom membrane system is to speed up the simulation as discussed in Chapter 2. However, it is important to perform analysis on the interaction and structures using an all-atom build considering the HMMM is not an accurate representation of the IM. Converting back to the all-atom and then continuing to perform MD allows for the IM to react naturally to the peptide. Figure 5.2 shows the final binding locations of the all-atom MD simulations after 150 ns. The objective of analyses for the combined system was to observe any structural changes in the peptide in the presence of the lipid bilayer and to observe any structural changes to the IM as a result of peptide presence. We also hoped to detail the location of the peptide with respect to the IM and if any penetration exists, to measure the level of penetration into the hydrophobic core.

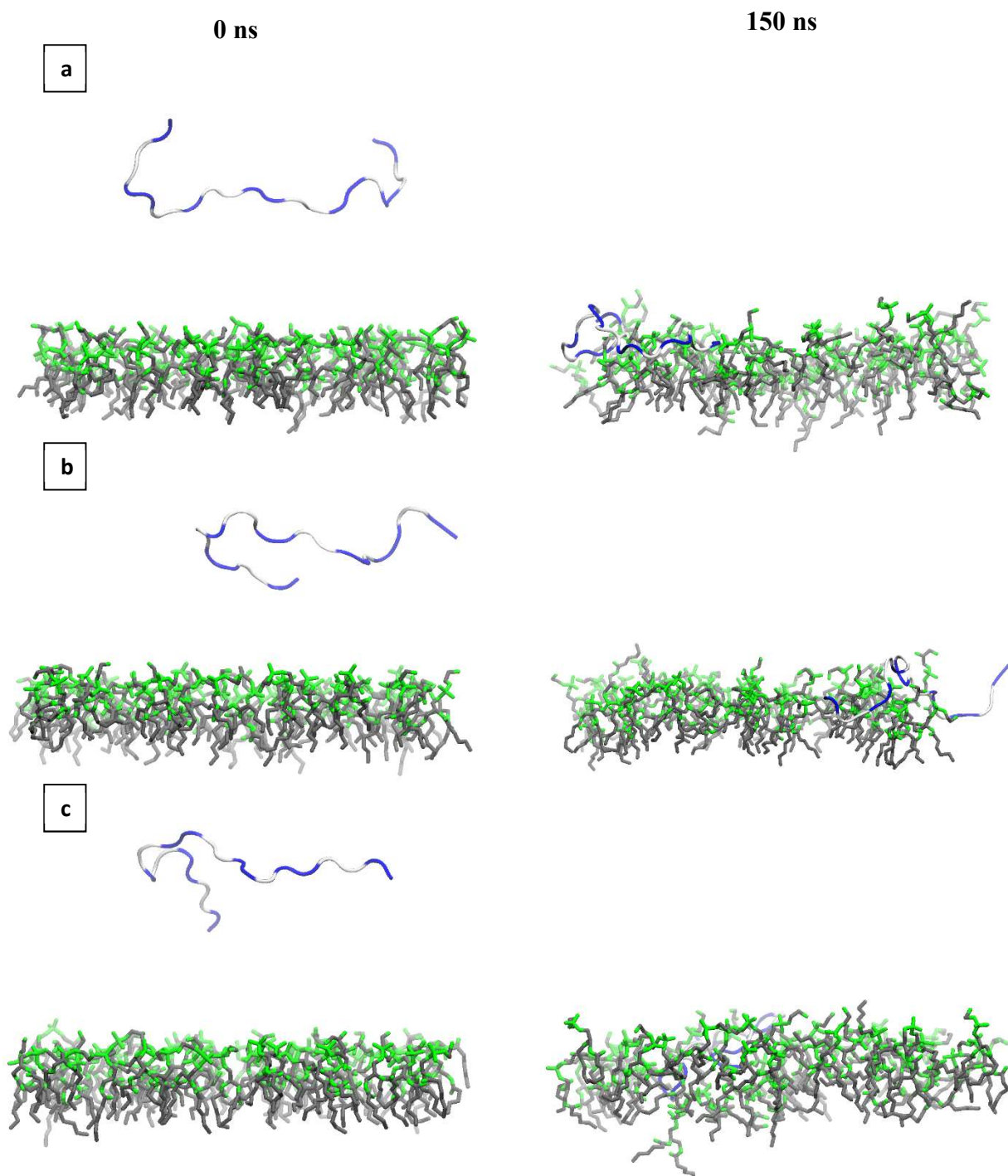


Figure 5.1 HMMM binding mechanisms including initial placement (left) and after 200 ns of MD (right) for **(a)** system 1 **(b)** system 2 **(c)** system 3. Lipids shown without hydrogen and with the naming color scheme; carbon tail (gray) and phosphate headgroup (green). Peptide colored by residue; non-polar (white) and polar (blue).

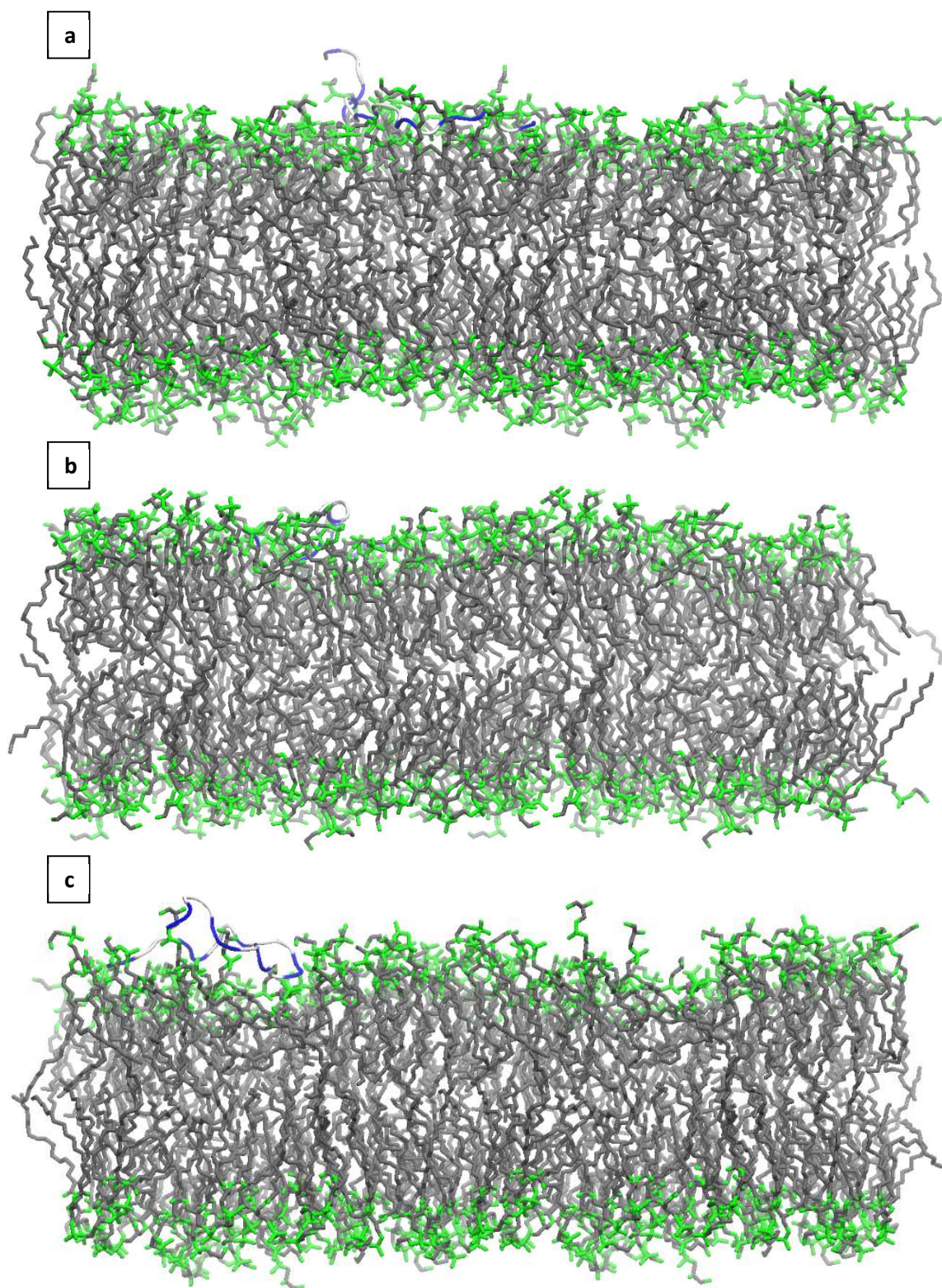


Figure 5.2 Unstructured WLBU2-mod with all-atom IM after 150 ns of MD (a) system 1 (b) system 2 (c) system 3. Lipids shown without hydrogen and with the naming color scheme; carbon tail (gray) and phosphate headgroup (green). Peptide colored by residue; non-polar (white) and polar (blue).

Using snapshots helps define a baseline of the location of the peptide but it is important to quantify in more atomistic detail the location of the peptide with respect to the IM. Figure 5.3 shows the EDP for the three systems. The focus of this analysis is to detail where the peptide is with respect to the density of the IM, therefore, the carbon groups of the lipid tails have been left out to highlight the peptide density. In all three systems the EDP shows a dip in the density for the upper leaflet where the peptide was introduced. The presence of the peptide disperses the headgroups toward the bilayer center as it maintains its structural integrity in separating the hydrophobic core and the water surrounding the upper-leaflet of the IM. Most of the peptide density exists within or just outside of the headgroups of the lipids without showing evidence of penetration past the headgroups into the hydrophobic core. The phosphate groups are still predominantly in the same location as the lower-leaflet and the IM control simulation, however, the density peak values have decreased slightly indicating some displacement centralized around the peak locations. The control IM upper-leaflet phosphate groups had a peak location of 20.3 Å and a peak density value average of 0.1125 ± 0.0008 Å while the IM with WLBU2-mod had a peak location also of 20.3 Å but a density peak value average of 0.0978 ± 0.0013 Å. The glycerol and carbonyl groups moved slightly toward the bilayer center and the density peak values decreased in a similar fashion to the phosphate groups. The control carbonyl atoms had an average location of 15.97 Å on the upper-leaflet and a peak density average of 0.0652 ± 0.0003 Å while the IM with WLBU2-mod had an average location of 15.83 Å and a peak density average of 0.0567 ± 0.0011 Å. The control glycerol atoms had an average location of 17.03 Å and a peak density average of 0.0761 ± 0.0006 Å while the IM with WLBU2-mod had an average location of 16.90 Å and a peak density average of

$0.0680 \pm 0.0009 \text{ \AA}$. The carbonyl and glycerol atoms were pushed toward the bilayer center slightly with a displacement of atom density throughout the headgroup region. This is most likely a result of the carbonyl and glycerol atoms resisting contact with the cationic residues of the peptide. We do not see any indication of the peptide density beyond the headgroup atoms. The headgroup displaces in response to the peptide while some atoms are pushed toward the bilayer center, but the overall structure of the headgroup remains intact and the peptide density is primarily outside of the acyl chain.

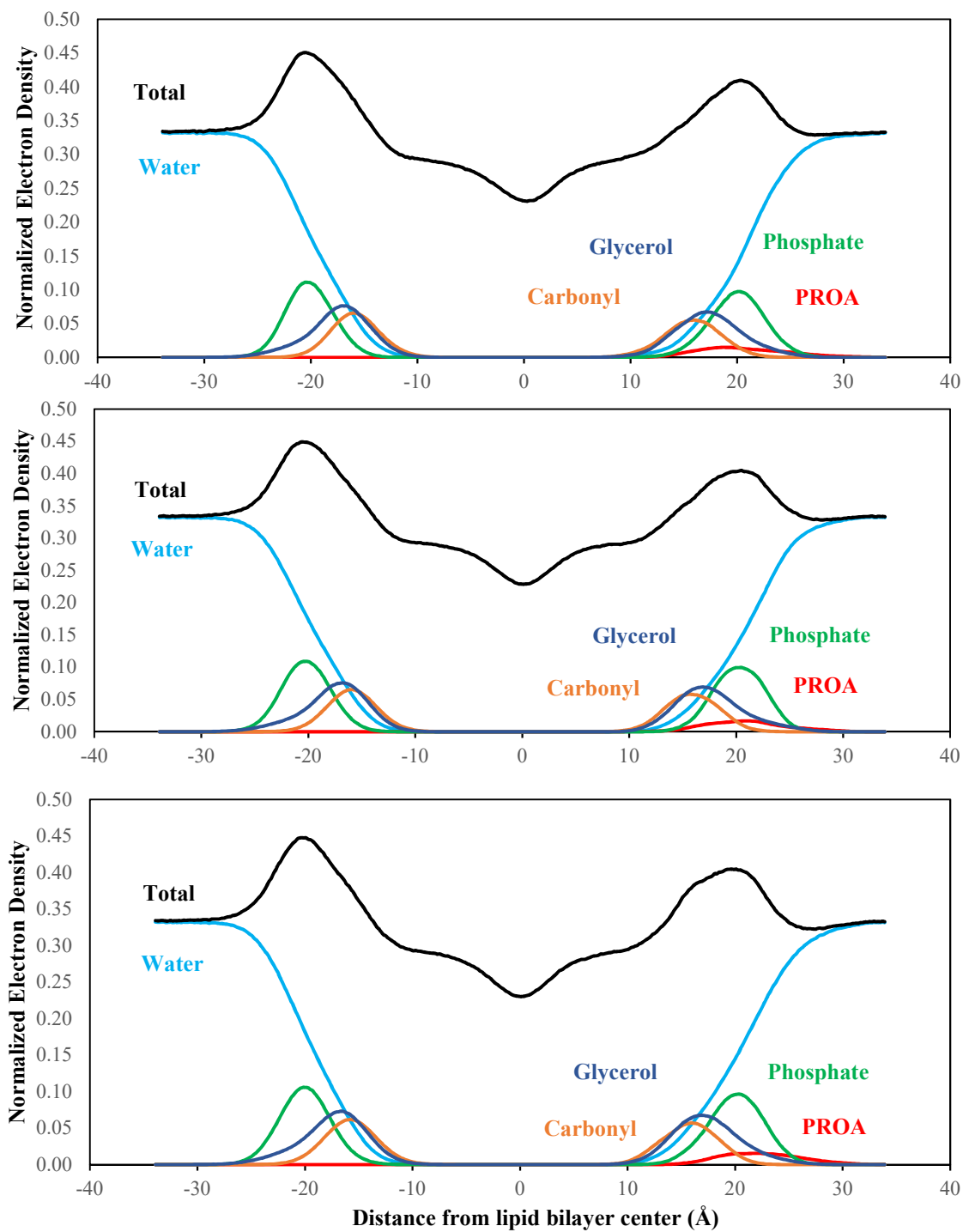


Figure 5.3 Electron Density Profile for the three all-atom systems with unstructured WLBU2-mod and IM after 150 ns of MD simulation.

After considering the densities of the atom groups for both the IM and the peptide, it is also important to look at how the introduction of the peptide influences the order of the lipid tails. The peptide does not penetrate the hydrophobic core in our simulations so it is easy to imagine the order parameters will not deviate much compared to the control simulation without the peptide. In comparing Figure 5.4 to Figure 4.5, we see almost no change in the order for the PE lipids. However, whereas before we saw slightly higher order for PG lipids, now with the presence of the peptide we see slightly less order for PG for the ordered index closest to the headgroup. As expected, the order for both PE and PG lipids remains unchanged near the bilayer center where the peptide has little influence on order and structure. The chain order decrease for PG lipids could be a result of interactions between the amino group and the peptide since this is the major structural change between POPE and POPG. The experimental NMR results collected and analyzed by Drs. Anja Penk and Daniel Huster for the IM with WLBU2 can also be seen in Figure 5.4. As with the control, the experimental order parameters are significantly lower than the simulation results. This was explained for the control IM to be caused by the experimental increase in temperature. The experiments were carried out at 310 K, while MD simulations were performed at 303 K. This increase in temperature also helps explain some of the difference for the IM with the peptide. However, we see increased disparity toward the mid-level order between experimental and simulation results. This is expected considering experimental observations indicate a degree of bilayer thinning that simulations have not been able to replicate. Bilayer thinning would suggest some degree of penetration into the hydrophobic core. The penetration of the peptide in experiments would cause decreased

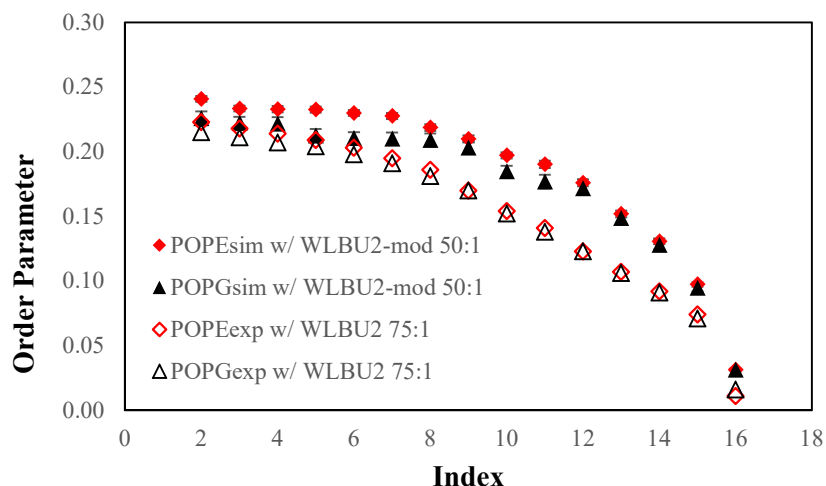


Figure 5.4 Chain order parameters for POPE and POPG with unstructured WLBU2-mod. Simulation data were re-ordered to match NMR assumption of monotonically decreasing order parameters. Simulation data taken from equilibrated region of the three all-atom IM replicas simulated at 303 K. Experimental data collected via NMR at 310 K by Drs. Anja Penk and Daniel Huster.

order near the bilayer center and without the same level of penetration in simulations the same disorder cannot be replicated.

The structure of the peptide in the presence of the IM seems to have no correlation to conforming to any specific secondary structure. The peptide was introduced to the IM after unfolding as a result of REST2. The resulting structures of REST2 consisted of 16%-20% α -helical character. After 150 ns of MD simulation with the HMMM IM mimic and then another 150 ns of MD simulation with the full lipid system we found the resulting secondary structure makeup of the peptides to vary. System 1 had a slight decrease in α -helical character to 18%, system 2 decreased drastically to 12% α -helical character, and system 3 increased to 28% α -helical character. This is most likely a result of the peptide placement along the bilayer-water interface that results in a peptide in various conformations. The peptide seems to be reacting to the electrostatic interactions between

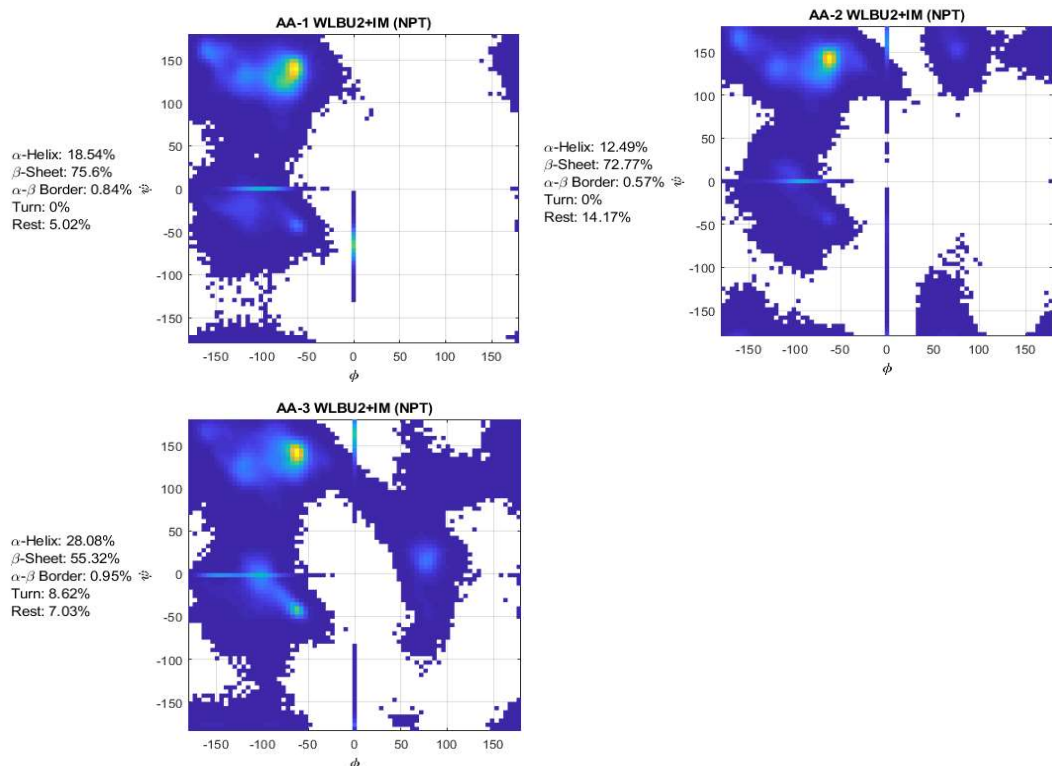


Figure 5.5 Ramachandran plots of the three all-atom systems with unstructured WLBU2-mod and IM after 150 ns of MD simulation.

the negatively charged lipid headgroup and its own cationic makeup which results in various conformations.

We demonstrated in Chapter 3 with experimental CD results that WLBU2 in an aqueous environment is primarily unstructured with a majority of its structure made of random coil and β -sheet characteristics. Early in the project, intermediate CD results of WLBU2 with the IM suggested the peptide to be unstructured, similar to the peptide in water. However, these results were considered erroneous and new CD experiments were performed and revealed that the peptide with the IM is primarily α -helical. Figure 5.6 shows the experimental CD data of WLBU2 with the gram-negative IM, collected and analyzed by Aria Salyapongse and Dr. Tristram-Nagle. Based on the intermediate CD results as well as the CD results of the peptide in water, REST2 was performed in ordered

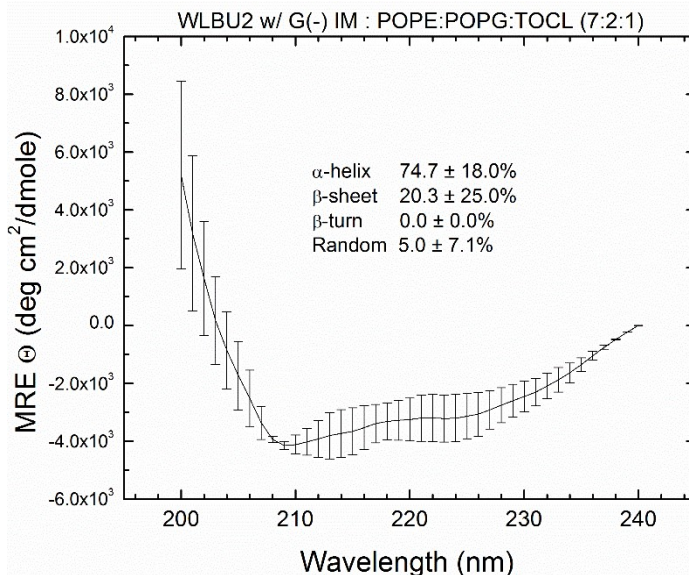


Figure 5.6 Experimental CD of WLBU2 with the gram-negative IM. CD taken by Aria Salyapongse and analyzed by Aria Salyapongse and Dr. Tristram-Nagle.

to match our peptide structure to experimental results. However, in light of the up-to-date experimental CD data, we decided to also perform MD simulations involving the original Robetta^{5, 6} predicted structures with the IM. The original Robetta^{5, 6} predicted structures, both single-helix and double-helix, have > 70% α -helical character and are most similar to the conformation seen in experiments for WLBU2 with the IM. The next section focuses on the analysis and discussion of the MD simulations involving the structured peptides with the IM.

5.2 Results of Structured WLBU2-mod and IM

Based on the up-to-date CD experiments indicating a structured α -helical peptide in the presence of the IM, we decided to perform MD simulations including the original Robetta predicted structures with the IM. The peptide structure in these simulations are a pure structure prediction (no relaxation based on MD or REST2 has been performed).

Three replicas of each Robetta^{5, 6}-predicted structure were combined with a HMMM IM mimic and we performed 150 ns of brute force MD. The binding motifs were

considered observationally, and a single system of each structure was chosen to be converted to an all-atom system where an additional 150 ns of MD was performed. Figure 5.7 shows the initial (0 ns) placement of the peptide with the HMMM systems and the binding locations after 150 ns. As with the unstructured WLBU2-mod systems, binding with the IM occurred within a few nanoseconds of MD. Figure 5.8 shows the final binding location after 150 ns of MD after the systems were converted to an all-atom lipid system. After 150 ns of MD with the HMMM IM and then conversion to a full-lipid system and another 150 ns of MD, both the double-helix and single-helix peptides maintained their structure without losing any α -helical character. We saw changes in the structure of the unstructured peptides because the extended structure can easily conform to different motifs as a result of electrostatic interactions with the anionic headgroups. The structured peptides have significantly more hydrogen bonding and electrostatic interactions holding the structure together and this results in almost no structural change when in the presence of the IM.

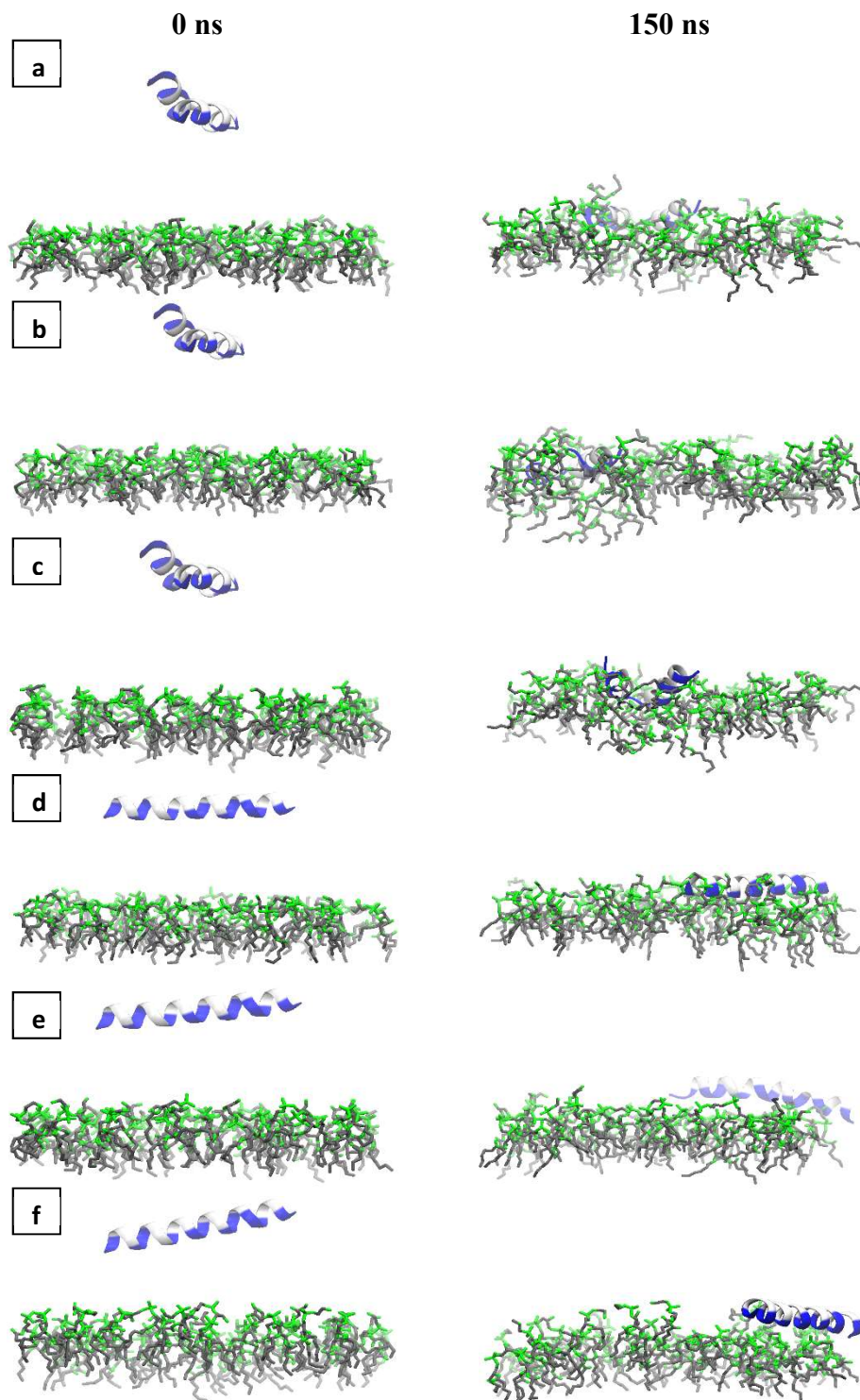


Figure 5.7 HMMM binding mechanisms including initial placement (left) and after 150 ns of MD (right) for **(a-c)** double-helix **(d-f)** single-helix. Lipids shown without hydrogen and with the naming color scheme; carbon tail (gray) and phosphate headgroup (green). Peptide colored by residue; non-polar (white) and polar (blue).

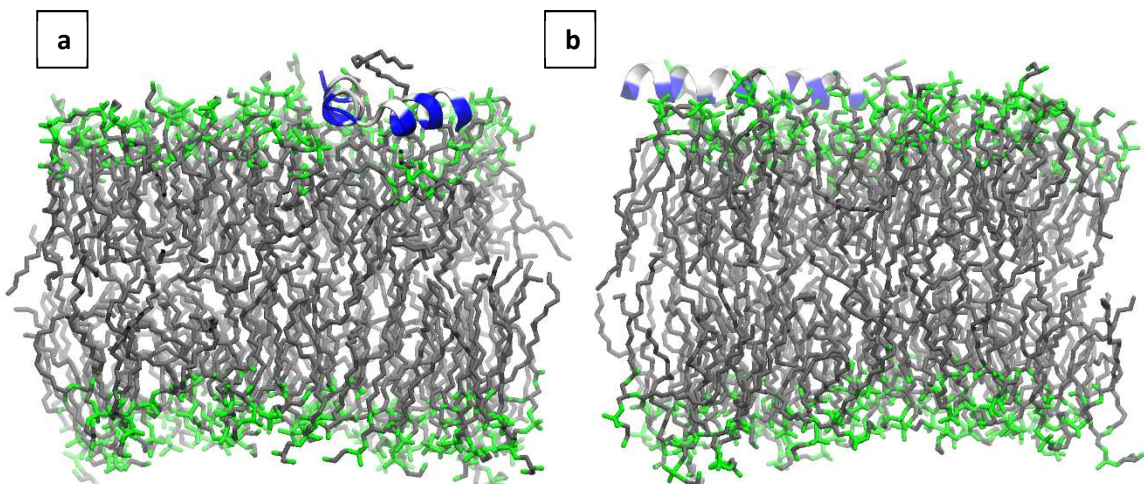


Figure 5.8 Structured WLBU2-mod with all-atom IM after 150 ns of MD (a) double-helix (b) single-helix. Lipids shown without hydrogen and with the naming color scheme; carbon tail (gray) and phosphate headgroup (green). Peptide colored by residue type; non-polar (white) and polar (blue).

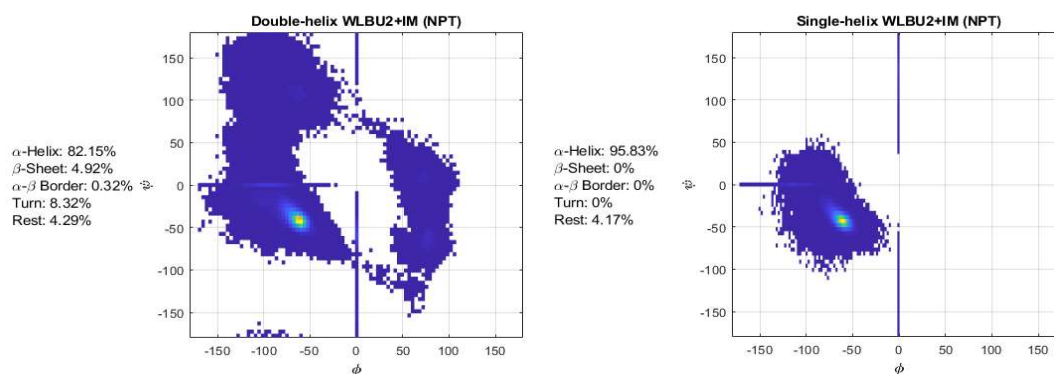


Figure 5.9 Ramachandran plots of structured WLBU2-mod with the all-atom IM after 150-ns of MD.

The EDP for the structured systems gives significant insight for comparing with each other as well as comparing with the unstructured systems and experimental results. The overall EDPs shown for both the double-helix and single-helix Robetta^{5, 6} predicted structures are shown in Figure 5.10. As with the unstructured peptide EDPs, we again see the loss of electron density in the headgroup region for the upper-leaflet in response to the addition of the peptide. The cationic Arg residues are pushing the hydrophobic carbonyl and glycerol atom groups toward the bilayer center while primarily dispersing the atom

densities in the headgroup. Looking at Figure 5.8 which shows the orientation of WLBU2-mod to have the non-polar residues facing the water, we can understand that the cationic portions of WLBU2 are the primary driving force for the interactions with the anionic headgroups of POPG and TOCL2. Such interactions are evident in the EDP where we see the peptide overlaps with the anionic headgroup region of the bilayer. Figure 5.11 shows the density peak locations for the double-helix and single-helix peptides. Clearly, the double-helix peptide exhibits a deeper level of penetration and interaction than the single-helix. However, when comparing the double-helix density location to the unstructured peptides discussed in the previous section, we fail to observe any deeper penetration. The single-helix is a rigid straight helical structure with strong steric hindrance. This steric hindrance could be the cause of its failure to completely interact with the headgroup and match the level of penetration seen by the double-helix conformation which has significantly less steric hindrance due to its β -turn characteristics. Unfortunately, for both the single-helix and double-helix peptides we fail to see any penetration into the hydrophobic core.

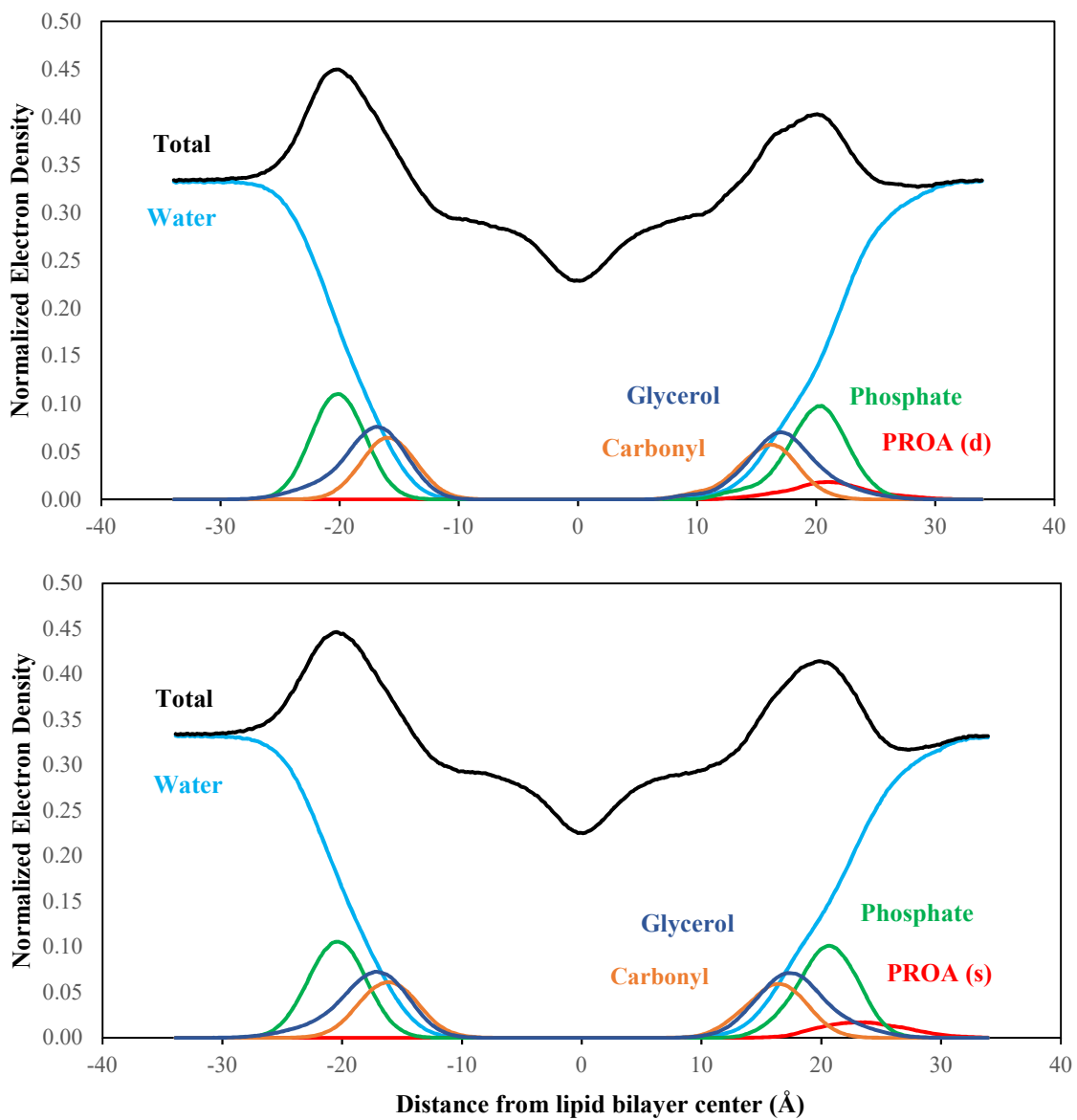


Figure 5.10 EDP for all-atom IM with structured WLBU2-mod after 150 ns of MD simulation. The first EDP is shown for the double-helix (d) conformation and the second EDP is shown for the single-helix (s) conformation.

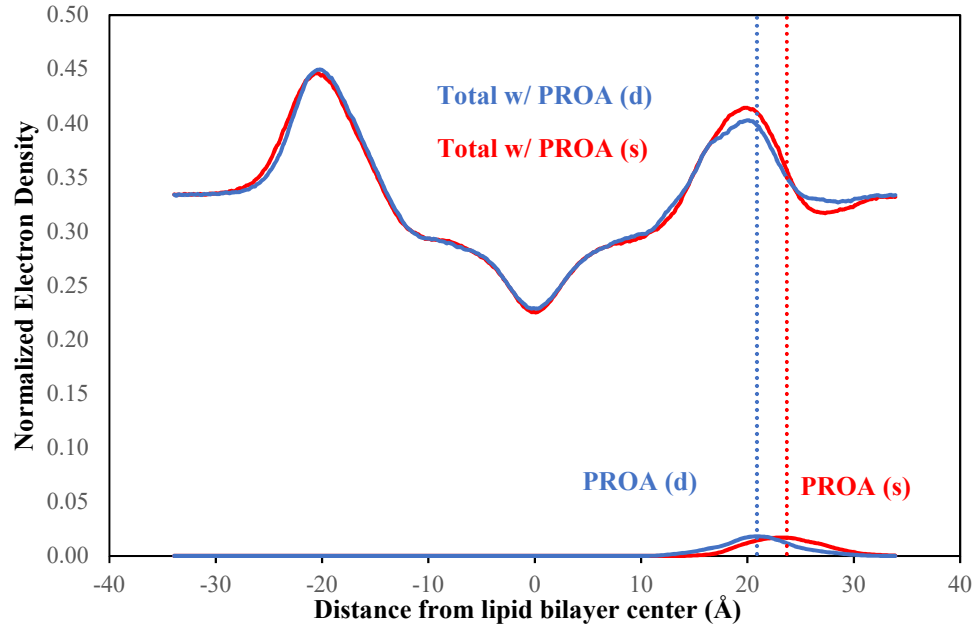


Figure 5.11 Electron density profile for the double-helix and single-helix structured WLBU2-mod with the IM. The dotted lines show where along the z-axis the maximum density for each structure occurs.

Aria Salyapongse and Dr. Tristram-Nagle have collected and prepared X-ray form factors for WLBU2 with the gram-negative IM in a 75:1 lipid/peptide ratio. The experimental results along with the simulation form factors for both the single-helix and double-helix structures are shown in Figure 5.12. From these form factors, we find the experimental results and our simulation results are not in complete agreement. The shift to higher q_z values for the experimental results indicate a larger surface area per lipid for the IM. This indicates some degree bilayer thinning experimentally. The same degree of bilayer thinning is not observed in our simulations as shown in both the simulation form factors as well as the snapshots and density profiles discussed previously. The double-helix FF is shifted to a slightly higher q_z value compared to the single-helix FF which can be explained by evidence of the double-helix structure exhibiting deeper penetration than the single-helix structure.

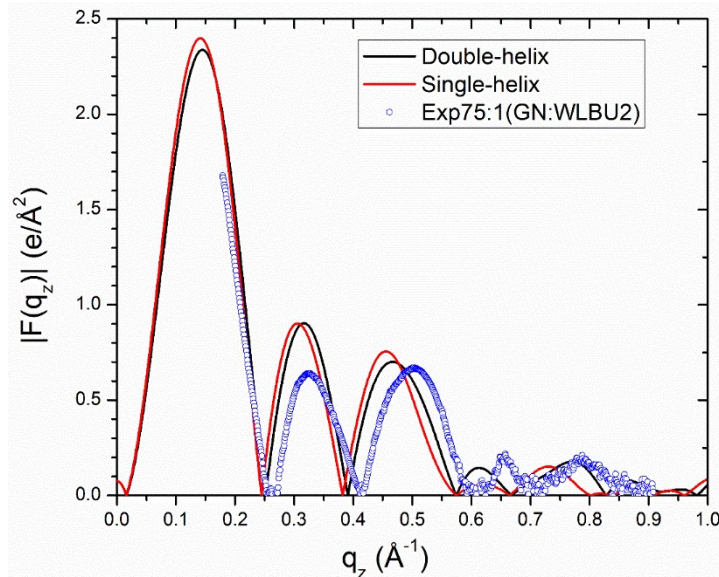


Figure 5.12 Form factors for MD simulations of double-helix and single-helix WLBU2-mod with gram-negative IM. Experimental IM X-ray form factor with WLBU2 taken and analyzed by Aria Salyapongse and Dr. Tristram-Nagle.

However, even this slight shift does not match the experimental shift which indicates bilayer thinning on a level that neither simulation matches. Whereas before we saw good agreement between the experimental and simulation for the form factors without the peptide, due to the lack of bilayer thinning in our simulations, we no longer see agreement when we introduce the peptide.

As shown through the experimental form factors, there is evidence of bilayer thinning in experiments that we do not see in our simulations. As such, it is reasonable to understand the difference in our chain order parameters between experimental and simulation results. The experimental control chain order parameters were significantly lower than the simulation order parameters due to the increase in temperature for the experimental NMR setup. Here we see the same effect but an increased disparity with the low-level order index. This is expected considering experiments observe bilayer thinning which would decrease lipid chain order. We also see that the simulated order parameters

for the double-helix structure are slightly lower than the single-helix which could be explained possibly by the slightly deeper penetration into the headgroup region by the double-helix peptide. As with the unstructured peptide simulated order parameters, we see slightly lower order for the POPG lipids compared to the control order parameters where the POPG and POPE lipids had similar order. Although the difference may be insignificant, there may be some preference for WLBU2-mod to interact with POPG over POPE lipids. This is the case, at least in the headgroup region of the IM, as our simulations fail to see any peptide penetration into the hydrophobic core.

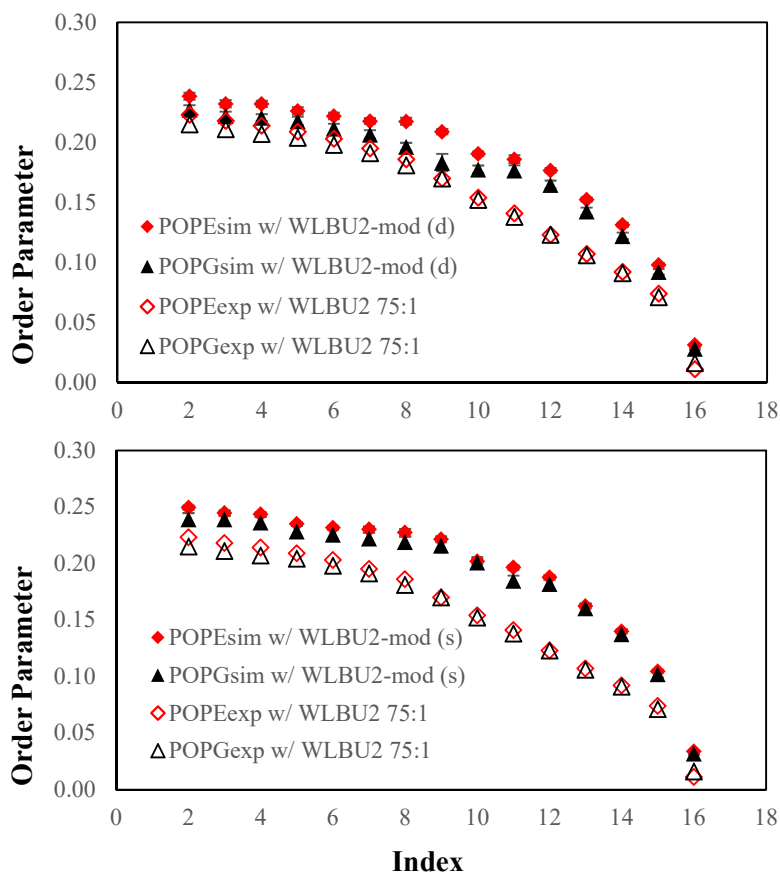


Figure 5.13 Chain order parameters for POPE and POPG with structured WLBU2-mod. The top panel shows the double-helix (d) and the bottom panel the single-helix (s) conformation. Simulation data were re-ordered to match NMR assumption of monotonically decreasing order parameters. Simulation data taken from equilibrated region of the all-atom IM simulated at 303 K. Experimental data collected via NMR at 310 K by Drs. Anja Penk and Daniel Huster.

CHAPTER 6: FINAL COMMENTS

6.1 Summary of Thesis

We started out with a peptide sequence with unknown structure. We used Robetta⁵,⁶ to help predict the structure and found two distinct possible candidates; a double-helix structure and a single-helix structure. Both conformations exhibited primarily an α -helical structure. From intermediate experimental CD results, we decided to perform MD on these peptide structures in the hope of converging to a uniform unstructured conformation. Due to high surface energy barriers for both systems, simplistic brute force MD methods failed, and we resorted to REST2 to help overcome the energy barriers. REST2 performed on both Robetta^{5, 6} predicted structures resulted in uniform unstructured conformations that were in agreement with experimental CD results for WLBU2 in an aqueous environment. We found the peptide after performing REST2 to lose most of the α -helical structure and conform to mostly random coil and β -sheet characteristics. Using quantifiable metrics such as RGY, ϕ and ψ backbone angles, and residue contacts, we were able to determine the most probable conformations from both Robetta^{5, 6} predicted structures to be used in simulations involving the IM. Simultaneously with simulations involving the peptide in water, we performed standard MD simulations on the gram-negative IM mimic using a 7:2:1 ratio of POPE:POPG:TOCL2. After considering both the peptide and the IM separately in explicit aqueous solvents, we placed the highly probable peptide structures above and in parallel with the IM mimics and observed the interaction as well as the resulting characteristic changes for both the peptide and IM. It was at this point in the project that the intermediate experimental CD results were taken to be erroneous and new CD measurements indicated that the peptide was mostly α -helical in the presence of the

IM. We decided to run additional simulations placing the original Robetta^{5, 6} predicted structures without relaxation via MD or REST2 above and in parallel with the IM. Our simulations showed little indication of significant bilayer thinning or penetration of the peptide into the hydrophobic core of the IM mimic. Experimental X-ray results did however observe bilayer thinning that our simulations were unable to match. The bilayer thinning shown in both the experimental X-ray FF and CD results could suggest some degree of penetration, but more analysis will be required to confirm. The next section will cover in more detail the positive takeaways as well as the shortcomings of the work presented here and present potential solutions to resolve the disagreement between simulation and experimental work for future projects to consider.

6.2 Final Comments and Future Work

Our simulation work in collaboration with Dr. Tristram-Nagle's experimental work had some agreement and some disagreement. Experimental CD results for WLBU2 in water indicate the structure of WLBU2 to be mostly random coil with significant β -sheet characteristics. After forgoing brute-force MD and turning to REST2 to allow the peptide to converge to a uniform unstructured conformation, we found the resulting structures to be in agreement with experimental CD results. Experimental CD results for WLBU2 with the IM indicate the peptide to be mostly structured with primarily α -helical secondary structure. Robetta^{5, 6} appears to predict the structure for WLBU2 consisting of primarily α -helical secondary structure with two potential structural make-ups; double-helix and single-helix conformations. Unfortunately, the work presented in this thesis was unable to significantly agree with what experiments found for the interactions between the peptide and the IM. Even though the peptide structure was predicted with secondary structure

make-up consistent with experimental CD results, the degree of membrane thinning found in experiments could not be matched with the simulation setup and timescales used in this thesis. Experimental X-ray FF and NMR data found significant bilayer thinning which would suggest penetration of WLBU2 into the hydrophobic core of the IM, where our simulations observed primary interactions with the headgroups and a failure to penetrate the hydrophobic core.

There are several options for continuing this project in the hopes of matching experimental results. The first, HMMM builds of the double-helix and single-helix systems could be run for a longer time-scale in the hopes of seeing a deeper penetration past the headgroup before converting to an all-atom lipid system, which could lead to chain perturbation and membrane thinning. Second, Figure 5.8 shows that the non-polar residues of WLBU2-mod are facing away from the bilayer. These residues are crucial for interacting with the hydrophobic tails of the IM and perhaps the orientation of WLBU2-mod could be flipped to have these residues face the bilayer. The swap in orientation might allow for a different mechanism of attack than we currently see with the cationic residues facing the bilayer. The primary driving force of the initial mechanism of interaction are the electrostatic interactions between the cationic residues of WLBU2-mod and the anionic headgroups of the IM. By flipping the orientation of the peptide and having the cationic residues face away from the bilayer, that primary driving force may cause the peptide to penetrate deeper into the IM as it attempts to align the positive residues with the negative atoms of the IM. There is evidence that the simulations presented here could be intermediate states toward the correct binding mechanisms. By allowing the simulations to run for a longer time or utilize different peptide placements and orientations we could

potentially see our simulations continue toward the correct binding sequence and observe penetration that experimental results suggest. A third option would be to forcibly pull one terminus of the peptide into the hydrophobic core past the headgroup and continue to perform MD on this forced system. Forcibly pulling the molecule is not ideal as it does not depict a natural interaction but doing-so could give atomistic insight into how the peptide would interact with the IM once past the headgroups.

It was demonstrated earlier that the mistake in the peptide sequence that was used for all simulations discussed in this thesis was found to be insignificant in the structure prediction of the peptide. However, if all future potential methods discussed are insufficient in demonstrating experimental levels of penetration of the IM, perhaps the final consideration could be to reconstruct the MD simulations using the correct WLBU2 sequence. Hopefully, using some of the methods discussed will result in good agreement with experimental results and can help give insight toward developing WLBU2 as a potentially new antibacterial therapeutic in the wake of the resistant crisis we face today.

REFERENCES

1. Bahar, A. A.; Ren, D., Antimicrobial Peptides. *Pharmaceuticals (Basel)* 2013, 6 (12), 1543-75.
2. Brogden, K., Antimicrobial peptides: Pore formers or metabolic inhibitors in bacteria? In *Nature Reviews Microbiology*, 2005; Vol. 3, pp 238-250.
3. Ventola, C. L., The Antibiotic Resistance Crisis: Part 1: Causes and Threats. In *Pharmacy and Therapeutics*, 2015; Vol. 40, pp 277-83.
4. Smith, P. A.; Koehler, M. F. T.; Girgis, H. S.; Yan, D.; Chen, Y.; Chen, Y.; Crawford, J. J.; Durk, M. R.; Higuchi, R. I.; Kang, J.; Murray, J.; Paraselli, P.; Park, S.; Phung, W.; Quinn, J. G.; Roberts, T. C.; Rougé, L.; Schwarz, J. B.; Skippington, E.; Wai, J.; Xu, M.; Yu, Z.; Zhang, H.; Tan, M.-W.; Heise, C. E., Optimized arylomycins are a new class of Gram-negative antibiotics. *Nature* 2018, 561 (7722), 189.
5. Raman, S.; Vernon, R.; Thompson, J.; Tyka, M.; Sadreyev, R.; Pei, J.; Kim, D.; Kellogg, E.; DiMaio, F.; Lange, O.; Kinch, L.; Sheffler, W.; Kim, B. H.; Das, R.; Grishin, N. V.; Baker, D., Structure prediction for CASP8 with all-atom refinement using Rosetta. *Proteins* 2009, 77 (0 9), 89-99.
6. Song, Y.; DiMaio, F.; Wang, R. Y. R.; Kim, D.; Miles, C.; Brunette, T.; Thompson, J.; Baker, D., High resolution comparative modeling with RosettaCM. *Structure* 2013, 21 (10).
7. Jo, S.; Kim, T.; Iyer, V. G.; Im, W., CHARMM-GUI: A web-based graphical user interface for CHARMM. *Journal of Computational Chemistry* 2008.
8. Jo, S.; Cheng, X.; Islam, S. M.; Huang, L.; Rui, H.; Zhu, A.; Lee, H. S.; Qi, Y.; Han, W.; Vanommeslaeghe, K.; Jr., A. D. M.; Roux, B.; Im, W., Chapter Eight - CHARMM-GUI PDB Manipulator for Advanced Modeling and Simulations of Proteins Containing Nonstandard Residues. *Advances in Protein Chemistry and Structural Biology* 2014, 96, 235-265.
9. Jorgensen, W. L.; Chandrasekhar, J.; Madura, J. D.; Impey, R. W.; Klein, M. L., Comparison of simple potential functions for simulating liquid water. *The Journal of Chemical Physics* 1983.
10. Huang, J.; MacKerell, A. D., Jr., CHARMM36 all-atom additive protein force field: validation based on comparison to NMR data. *Journal of Computational Chemistry* 2013, 34 (25), 2135-45.
11. Wang, L.; Friesner, R.; Berne, B., Replica Exchange with Solute Scaling: A More Efficient Version of Replica Exchange with Solute Tempering (REST2). *Physical Chemistry* 2011, 115.
12. Huang, J.; Rauscher, S.; Nawrocki, G., CHARMM36m: an improved force field for folded and intrinsically disordered proteins. *Nature Methods* 2017, 14.
13. Brooks, B. R.; Brooks, C. L., 3rd; Mackerell, A. D., Jr.; Nilsson, L.; Petrella, R. J.; Roux, B.; Won, Y.; Archontis, G.; Bartels, C.; Boresch, S.; Caflisch, A.; Caves, L.; Cui, Q.; Dinner, A. R.; Feig, M.; Fischer, S.; Gao, J.; Hodoscek, M.; Im, W.; Kuczera, K.; Lazaridis, T.; Ma, J.; Ovchinnikov, V.; Paci, E.; Pastor, R. W.; Post, C. B.; Pu, J. Z.; Schaefer, M.; Tidor, B.; Venable, R. M.; Woodcock, H. L.; Wu, X.; Yang, W.; York, D. M.; Karplus, M., CHARMM: the biomolecular simulation program. *Journal of Computational Chemistry* 2009, 30 (10), 1545-614.
14. Hovmöller, S.; Zhou, T.; Ohlson, T., Conformations of amino acids in proteins. *Acta Crystallographica Section D* 2002.
15. Humphrey, W.; Dalke, A.; Schulten, K., VMD: visual molecular dynamics. *Journal of Molecular Graphics* 1996, 14 (1), 33-8, 27-8.
16. Wu, E. L.; Cheng, X.; Jo, S.; Rui, H.; Song, K. C.; Dávila-Contreras, E. M.; Qi, Y.; Lee, J.; Monje-Galvan, V.; Venable, R. M.; Klauda, J. B.; Im, W., CHARMM-GUI Membrane Builder toward realistic biological membrane simulations. *Journal of Computational Chemistry* 2014.

17. Lee, J.; Patel, D. S.; Ståhle, J.; Park, S.-J.; Kern, N. R.; Kim, S.; Lee, J.; Cheng, X.; Valvano, M. A.; Holst, O.; Knirel, Y. A.; Qi, Y.; Jo, S.; Klauda, J. B.; Widmalm, G.; Im, W., CHARMM-GUI Membrane Builder for Complex Biological Membrane Simulations with Glycolipids and Lipoglycans. *Journal of Chemical Theory and Computation* 2018.
18. Jo, S.; Kim, T.; Im, W., Automated Builder and Database of Protein/Membrane Complexes for Molecular Dynamics Simulations. *PLoS ONE* 2007.
19. Jo, S.; Lim, J. B.; Klauda, J. B.; Im, W., CHARMM-GUI Membrane Builder for Mixed Bilayers and Its Application to Yeast Membranes. *Biophysical Journal* 2009, 97 (1), 50-58.
20. Klauda, J. B.; Venable, R. M.; Freites, J. A.; O'Connor, J. W.; Tobias, D. J.; Mondragon-Ramirez, C.; Vorobyov, I.; MacKerell, A. D., Jr.; Pastor, R. W., Update of the CHARMM all-atom additive force field for lipids: validation on six lipid types. *Journal of Physical Chemistry B* 2010, 114 (23), 7830-43.
21. Qi, Y.; Cheng, X.; Lee, J.; Park, S.; Klauda, J. B.; Im, W., CHARMM-GUI HMMM Builder for Membrane Simulations with the Highly Mobile Membrane-Mimetic Model. *Biophysical Journal* 2015.
22. Wildermuth, K.; Monje-Galvan, V.; Warburton, L.; Klauda, J., Effect of Membrane Lipid Packing on Stable Binding of the ALPS Peptide. *Journal of Chemical Theory and Computation* 2019, 15.
23. Brahms, S.; Brahms, J., Determination of protein secondary structure in solution by vacuum ultraviolet circular dichroism. *Journal of Molecular Biology* 1980, 138 (2), 149-78.
24. Sohlenkamp, C.; Geiger, O., Bacterial membrane lipids: diversity in structures and pathways. *FEMS Microbiology Reviews* 2016, 40 (1), 133-159.
25. Parkin, J.; Chavent, M.; Khalid, S., Molecular Simulations of Gram-Negative Bacterial Membranes: A Vignette of Some Recent Successes. *Biophysical Journal* 2015, 109 (3), 461-8.
26. Olofsson, G.; Sparr, E., Ionization Constants pKa of Cardiolipin. *PLoS ONE* 2013.